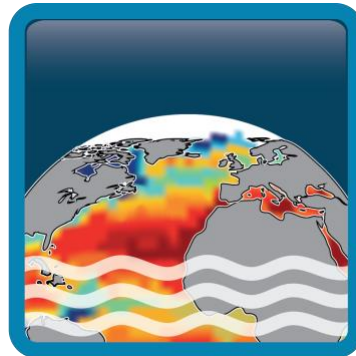


# Climate Change Initiative+ (CCI+) Phase 1

## Sea Surface Salinity



### Algorithm Development Plan (ADP)

**Customer:** ESA

**Ref.:** ESA-CCI-PRGM-EOPS-SW-17-0032

**Version:** v3.1

**Ref. internal:** AO/1-9041/17/I-NB\_v1r1





**Revision Date:** 14/09/2021

**Filename:** SSS\_cci-D2.4-ADP\_v3.1.docx





## Signatures

Author	Nicolas Reul (Science Leader)		14/09/2021
Reviewed by	Rafael Catany		
Approved by	Jacqueline Boutin (Science Leader)		14/09/2021
	Nicolas Reul (Science Leader)		14/09/2021
	Rafael Catany (Project Manager)		14/09/2021
Accepted by	Susanne Mecklenburg (Technical Officer) ESA		

Diffusion List
Sea Surface Salinity Team Members
ESA (Susanne Mecklenburg, Roberto Sabia, Paolo Cipollini)



## Amendment Record Sheet

Date / Issue	Description	Section / Page
16/07/2019 / v1.0	Circulation ADP year 1 to ESA	New document
29/11/2019 / v1.1	Revisions according to Paolo Cipollini comments. Added L-band evolution plan (section 2.3) and C-band development plan for year 2 (section 3).	Section 2.3 / page 7
19/12/2019 / v1.2	Amended text, to clarify that temporal resolution of SMOS and SMAP is of the order 3 days (not seconds).	Section 2.3.2 / page 9
14/09/2021 v3.1	Plan for L-band based algorithm development perspective for phase 2 has been added	Section 2.6 / page 13
	Summary of activities performed in year 3 for C/X-band based algorithm and perspective for phase 2 has been added	Section 3.4/ page 30
	Summary for phase-1 and perspective for phase-2 has been added	Section 4/page 31
	Published document (this document) including ESA feedback	N/A



## Table of Contents

<b>Signatures .....</b>	<b>iii</b>
<b>Amendment Record Sheet .....</b>	<b>v</b>
<b>List of figures .....</b>	<b>viii</b>
<b>List of tables .....</b>	<b>x</b>
<b>1 Introduction .....</b>	<b>1</b>
<b>1.1 Scope of this document .....</b>	<b>1</b>
<b>1.2 Structure of the document .....</b>	<b>1</b>
<b>1.3 References .....</b>	<b>1</b>
1.3.1 Applicable Documents.....	1
1.3.2 Reference Documents .....	1
<b>1.4 Acronyms.....</b>	<b>4</b>
<b>2 Plan for L-band data based CCI+SSS Algorithms.....</b>	<b>6</b>
<b>2.1 Input Level 2/Level 3 Data .....</b>	<b>6</b>
<b>2.2 Plan for L3 algorithms.....</b>	<b>6</b>
2.2.1 Input Data re-gridding .....	7
2.2.2 Space-time aggregation.....	7
<b>2.3 Plan for L4 algorithms.....</b>	<b>7</b>
2.3.1 Overview.....	7
2.3.2 Detailed plan for the level 4 algorithm steps .....	9
2.3.3 L4 products content.....	11
<b>2.4 Plan for the evolution of the L-band CCI algorithms for year 2 .....</b>	<b>12</b>
2.4.1 2 <sup>nd</sup> CRDP:.....	12
2.4.2 3 <sup>rd</sup> CRDP (2020-2021 period).....	13
<b>2.5 Plan for the evolution of the L-band CCI algorithms for year 3 .....</b>	<b>14</b>
<b>2.6 Plan for the evolution of the L-band CCI algorithms for phase 2 .....</b>	<b>15</b>
<b>3 Plan for C and X-band data based CCI SSS algorithm .....</b>	<b>17</b>
<b>3.1 Short overview of the physical principle of SSS retrieval from C- and X-band radiometer data</b>	<b>17</b>
<b>3.2 Algorithm Development plan.....</b>	<b>19</b>
<b>3.3 Summary of the activities performed in the first half of year 2 .....</b>	<b>23</b>
3.3.1 Updated Atmospheric Correction Algorithm .....	23
3.3.2 Empirical Adjustments.....	24
3.3.3 AMSRE SSS development Plan for end Year 2 and year 3.....	30
<b>3.4 Summary of the activities performed in year 3 and perspective for phase-2.....</b>	<b>32</b>
<b>4 Summary and way forward.....</b>	<b>33</b>

## List of figures

Figure 1: main L4 processing steps. -----	7
Figure 2 SST dependence of SSS bias for (red) SMOS and (blue) Aquarius. Bias is computed as differences between satellite SSS and Argo in situ measurements over the Aquarius era (Dinnat et al., 2019, <b>RD15</b> ). -----	13
Figure 3 Sensitivity of the flat ocean brightness temperature to SSS, namely, $\partial TB/\partial SSS$ as a function of electromagnetic frequency (x-axis) computed from Klein and Swift (1977) for the salinity of 35 psu and temperature of 15°C with a fixed incident angle of 53°. -----	18
Figure 4 Brightness temperature of sea surface in microwave bands as functions of SSS and SST. (a) brightness at 6.9 GHz (C band) (b) Brightness at 10.7 GHz (X band) in V-pol and (c) brightness temperature difference between the 10.7 GHz and 6.6 GHz in V-pol. -----	18
Figure 5 Sensitivity of $\Delta T_B = T_{B6.9V} - T_{B10.7V}$ to SSS & SST -----	20
Figure 6 Surface brightness temperature evolution as a function of surface wind speed for X-band channel in V-pol (red) and C-band channel in V-pol (black) -----	21
Figure 7 Oceanic Regions where SSS data shall be analyzed and produced using C/X band radiometer data -----	22
Figure 8 Brightness temperature calibration procedure for the SSS retrieval from AMSR-E or AMSR-2 radiometer data. The auxiliary data include SST, wind speed, cloud, liquid water, and water vapor used in the RTM. In KS model, SST is from GHRSSST and SSS from the CCI v1.8 dataset. -----	22
Figure 9: $T_v$ , representing a sea surface temperature that is typical for each water vapour value. -----	24
Figure 10: Wind-excess emissivity empirical GMF at C (a) and X (b) bands. The blue curves are showing the residual binned in 1 m/s binned $\pm 1$ STD. The red curves are showing the 4 <sup>th</sup> order polynomial fits used to define the algorithm GMF. -----	25
Figure 11: Flat surface emissivity residuals at C- (a) and X- (b) bands as function of the SST CCI. The blue curves are showing the residual binned in 1 m/s binned $\pm 1$ STD. -----	26
Figure 12: Observed residues of the differences between AMSRE surface emissivity at C-band and the forward model of the flat ocean surface emissivity forced with CCI SSS & SST data. The residuals are binned as function of water vapor (X-axis) and Cloud liquid water (Y-axis). Data were collected for 6 months over the four river plume regions. Right: Bi-dimensional 6th order polynomial fit. -----	26
Figure 13: Observed residues of the differences between AMSRE surface emissivity at X-band and the forward model of the flat ocean surface emissivity forced with CCI SSS & SST data. The residuals are binned as function of water vapor (X-axis) and Cloud liquid water (Y-axis). Data were collected for 6 months over the four river plume regions. Right: Bi-dimensional 6th order polynomial fit. -----	27



Figure 14: Monthly averaged (oct 2010) flat surface emissivity contrasts between C and X-bands (Top) from a flat ocean surface emissivity model forced by the SSS and SST CCI and (bottom) derived from AMSRE data using our algorithm. ----- 28

Figure 15: Monthly averaged (oct 2010) flat surface emissivity contrasts between C and X-bands derived from AMSRE data using our algorithm as compared to the flat ocean surface emissivity model forced by the SSS and SST CCI and (bottom).----- 29

Figure 16: Left: CCI SSS (color) observed in each bin of AMSR-E flat ocean surface emissivity (x-axis) and the CCI SST (y-axis). Right: 6 order polynomial fit of the data shown in a). ----- 30

Figure 17: Monthly averaged SSS in october 2010 in the Amazon-Orinoco River plume region from SSS L-band CCI (a) and SSS from C/X band AMSR-E (right). The thick contour represent the 35 isohaline. A regression plot of AMR-E vs L-band CCI SSS is shown in c). ----- 30

Figure 18: Monthly averaged SSS in February 2011 in the Congo-Niger River plume region from SSS L-band CCI (a) and SSS from C/X band AMSR-E (right). The thick contour represent the 35 isohaline. A regression plot of AMR-E vs L-band CCI SSS is shown in c). ----- 31

## List of tables

No table of figures entries found.



# 1 Introduction

## 1.1 Scope of this document

This document holds the Algorithm Development Plan (ADP) prepared by CCI+ team, as part of the activities included in the [WP210] of the Proposal (Task 2 from SoW ref. ESA-CCI-PRGM-EOPS-SW-17-0032).

This document summarizes the planned algorithm developments to be performed year 1-2 of the CCI+SSS project activity and prospective plans for the Phase-2 of the project.

## 1.2 Structure of the document

This document is composed of 4 sections and presents the plan for the development of the CCI-SSS algorithm that were proposed during year 1 and implemented during year 1 and 2, along to the evolution plan for year 2, and finally for year 3. **Section 1** is an introduction presenting the scope, reference and applicable documents, acronyms, and the structure of the document. **Section 2** presents the plan for the algorithms of the so-called Level 2 products which are swath retrieval, the Level 3 SSS products, which are averaged intermediate products obtained sensor by sensor without mixing inter-sensor information, and the Level 4 data set which is foreseen to be produced each year and form the core of the CCI-SSS products. In **Section 3**, we detail the algorithm development for CCI-SSS algorithms based on C and X-band data and in **section 4**, we provide summary and next steps.

## 1.3 References

### 1.3.1 Applicable Documents

ID	Document	Reference
AD01	CCI+ Statement of Work	SoW
AD02	Product User Guide (PUG)	PUG
AD03	User Requirement Document (URD)	SSS_cci-D1.1-URD-i1r0
AD04	Product Specification Document (PSD)	SSS_cci-D1.2-PSD-v1r4
AD05	Algorithm Theoretical Baseline Document	SSS_cci-D2.3-ATBD_L3_L4-i1r0_v1.1

### 1.3.2 Reference Documents

ID	Document	Reference
RD01	Boutin, J., N. Martin, N. Kolodziejczyk, and G. Reverdin (2016a), Interannual anomalies of SMOS sea surface salinity, <i>Remote Sensing of Environment</i>	doi:http://dx.doi.org/10.1016/j.rse.2016.02.053



**Climate Change Initiative+ (CCI+)**  
**Phase 1**  
**Algorithm Development Plan**

Ref.: ESA-CCI-PRGM-EOPS-SW-17-0032

Date: 14/09/2021

Version: v3.1

Page: 2 of 47

ID	Document	Reference
RD02	Kolodziejczyk, N., J. Boutin, J.-L. Vergely, S. Marchand, N. Martin, and G. Reverdin (2016), Mitigation of systematic errors in SMOS sea surface salinity, <i>Remote Sensing of Environment</i>	doi:http://dx.doi.org/10.1016/j.rse.2016.02.061.
RD03	Liang Hong, Normal Kuring, Joel Gales and Fred Patt (2017), AQ-014-PS-0017_Aquarius_L2toL3ATBD_DatasetVersion5.0	
RD04	Fred Patt, Liang Hong (2017), AQ-014-PS-0018_AquariusLevel2specification_DatasetVersion5.0	
RD05	Meissner, T. and F. J. Wentz, 2016: Remote Sensing Systems SMAP Ocean Surface Salinities [Level 2C, Level 3 Running 8-day, Level 3 Monthly], Version 2.0 validated release. Remote Sensing Systems, Santa Rosa, CA, USA.	www.remss.com/missions/smap, doi:10.5067/SMP20-2SOCS
RD06	Boutin J., J.-L. Vergely, S. Marchand, F. D'Amico, A. Hasson, N. Kolodziejczyk, N. Reul, G. Reverdin, J. Vialard (2018), New SMOS Sea Surface Salinity with reduced systematic errors and improved variability, <i>Remote Sensing Of Environment</i>	doi:http://dx.doi.org/10.1016/j.rse.2018.05.022
RD07	Yiwen Zhou ; Roger H. Lang ; Emmanuel P. Dinnat ; David M. Le Vine (2017), L-Band Model Function of the Dielectric Constant of Seawater, <i>IEEE Transactions on Geoscience and Remote Sensing</i> ( Volume: 55 , Issue: 12)	
RD08	Gaillard F. (2015), ISAS-13 temperature and salinity gridded fields. SEANOE.	http://doi.org/10.17882/45945.
RD09	Reul Nicolas, Saux Picart Stephane, Chapron Bertrand, Vandemark D., Tournadre Jean, Salisbury J. (2009). Demonstration of ocean surface salinity microwave measurements from space using AMSR-E data over the Amazon plume. <i>Geophysical Research Letters</i> ( GRL ) , 36, 1-5 .	https://doi.org/10.1029/2009GL038860
RD10	Qingtao Song and Zhaohui Wang. (2017). Sea surface salinity observed from the HY-2A satellite. <i>Satellite Oceanography and Meteorology</i> , vol.2 (1): 41–48.	http://dx.doi.org/10.18063/SOM.2017.01.004.
RD11	Wentz, F. J., and T. Meissner (2000), AMSR ocean algorithm, version 2, algorithm theoretical basis document, RSS Tech. Rep. 121599A-1, Remote Sens. Syst., Santa Rosa, Calif.	
RD12	Wentz, F. J. and T. Meissner, (2007), AMSR-E Ocean Algorithms; Supplement 1, report number 051707, 6 pp., Remote Sensing Systems, Santa Rosa, CA.	
RD13	Meissner, T., and F. J. Wentz, (2012), The emissivity of the ocean surface between 6 - 90 GHz over a large range of wind speeds and Earth incidence angles, <i>IEEE TGRS</i> , 50(8), 3004-3026.	
RD14	Webster, W. J., T. T. Wilheit, D. B. Ross, and P. Gloersen (1976), Spectral characteristics of the microwave emission from a wind-driven foam-covered sea, <i>J. Geophys. Res.</i> , 18, 3095–3099.	
RD15	Dinnat, E.P.; Le Vine, D.M.; Boutin, J.; Meissner, T.; Lagerloef, G. Remote Sensing of Sea Surface Salinity: Comparison of Satellite and In Situ Observations and Impact of Retrieval Parameters. <i>Remote Sens.</i> <b>2019</b> , <i>11</i> , 750.	



**Climate Change Initiative+ (CCI+)**  
**Phase 1**  
**Algorithm Development Plan**

**Ref.:** ESA-CCI-PRGM-EOPS-SW-17-0032

**Date:** 14/09/2021

**Version:** v3.1

**Page:** 3 of 47

ID	Document	Reference
<b>RD16</b>	Olivier, L., G. Reverdin, A. Hasson, and J. Boutin (2020), Tropical Instability Waves in the Atlantic Ocean: Investigating the Relative Role of Sea Surface Salinity and Temperature From 2010 to 2018, <i>Journal of Geophysical Research: Oceans</i> , 125(12), e2020JC016641, doi: <a href="https://doi.org/10.1029/2020JC016641">https://doi.org/10.1029/2020JC016641</a>	
<b>RD17</b>	Akhil, V. P., J. Vialard, M. Lengaigne, M. G. Keerthi, J. Boutin, J. L. Vergely, and F. Papa (2020), Bay of Bengal Sea surface salinity variability using a decade of improved SMOS re-processing, <i>Remote Sensing of Environment</i> , 248, 111964, doi: <a href="https://doi.org/10.1016/j.rse.2020.111964">https://doi.org/10.1016/j.rse.2020.111964</a> .	
<b>RD18</b>	Reverdin, G., et al. (2021), Formation and Evolution of a Freshwater Plume in the Northwestern Tropical Atlantic in February 2020, <i>Journal of Geophysical Research: Oceans</i> , 126(4), e2020JC016981, doi: <a href="https://doi.org/10.1029/2020jc016981">10.1029/2020jc016981</a> .	
<b>RD19</b>	Kerr, Y., et al. (2019), Low Frequency Passive Microwave User Requirement Consolidation Study, Issue 2, <i>Rep. SO-TN-CB-GS-0075</i> , CESBIO, Toulouse, <a href="https://mycore.core-cloud.net/index.php/s/Y3tpySnNhl9HWUH">https://mycore.core-cloud.net/index.php/s/Y3tpySnNhl9HWUH</a>	
<b>RD20</b>	Fournier, S., and T. Lee (2021), Seasonal and Interannual Variability of Sea Surface Salinity Near Major River Mouths of the World Ocean Inferred from Gridded Satellite and In-Situ Salinity Products, <i>Remote Sensing</i> , 13(4), 728.	
<b>RD21</b>	Yu, L., F. M. Bingham, T. Lee, E. P. Dinnat, S. Fournier, O. Melnichenko, W. Tang, and S. H. Yueh (2021), Revisiting the Global Patterns of Seasonal Cycle in Sea Surface Salinity, <i>Journal of Geophysical Research: Oceans</i> , 126(4), e2020JC016789, doi: <a href="https://doi.org/10.1029/2020JC016789">https://doi.org/10.1029/2020JC016789</a> .	
<b>RD22</b>	Bingham, F. M., S. Brodnitz, and L. Yu (2021), Sea Surface Salinity Seasonal Variability in the Tropics from Satellites, Gridded In Situ Products and Mooring Observations, <i>Remote Sensing</i> , 13(1), 110.	
<b>RD23</b>	Melnichenko, O., P. Hacker, N. Maximenko, G. Lagerloef, and J. Potemra (2016), Optimum interpolation analysis of Aquarius sea surface salinity, <i>Journal of Geophysical Research: Oceans</i> , 121(1), 602-616, doi: <a href="https://doi.org/10.1002/2015JC011343">https://doi.org/10.1002/2015JC011343</a> .	
<b>RD24</b>	Nardelli, B., R. Droghei, and R. Santoleri (2016), Multi-dimensional interpolation of SMOS sea surface salinity with surface temperature and in situ salinity data, <i>Remote Sensing of Environment</i> , 180, 392-402, doi: <a href="https://doi.org/10.1016/j.rse.2015.12.052">https://doi.org/10.1016/j.rse.2015.12.052</a> .	
<b>RD25</b>	Kolodziejczyk, N., M. Hamon, J. Boutin, J.-L. Vergely, G. Reverdin, A. Supply, and N. Reul (2021), Objective Analysis of SMOS and SMAP Sea Surface Salinity to Reduce Large-Scale and Time-Dependent Biases from Low to High Latitudes, <i>Journal of Atmospheric and Oceanic Technology</i> , 38(3), 405-421, doi: <a href="https://doi.org/10.1175/jtech-d-20-0093.1">10.1175/jtech-d-20-0093.1</a> .	
<b>RD26</b>	Boutin, J., J.-L. Vergely, E. P. Dinnat, P. Waldteufel, F. D'Amico, N. Reul, A. Supply, and C. Thouvenin-Masson (2021), Correcting Sea Surface Temperature Spurious Effects in Salinity Retrieved From Spaceborne L-Band Radiometer Measurements, <i>IEEE Transactions on Geoscience and Remote Sensing</i> , 59(9), 7256-7269, doi: <a href="https://doi.org/10.1109/tgrs.2020.3030488">10.1109/tgrs.2020.3030488</a> .	
<b>RD27</b>	Kao, H.-Y., G. S. E. Lagerloef, T. Lee, O. Melnichenko, T. Meissner, and P. Hacker (2018), Assessment of Aquarius Sea Surface Salinity, <i>Remote Sens.</i> , 10(9):1341.	
<b>RD28</b>	Fournier, S., T. Lee, X. Wang, T. W. K. Armitage, O. Wang, I. Fukumori, and R. Kwok (2020), Sea Surface Salinity as a Proxy for Arctic Ocean Freshwater Changes, <i>Journal of Geophysical Research: Oceans</i> , 125(7), e2020JC016110, doi: <a href="https://doi.org/10.1029/2020JC016110">https://doi.org/10.1029/2020JC016110</a> .	



ID	Document	Reference
<b>RD29</b>	Brucker, L., E. P. Dinnat, and L. S. Koenig (2014), Weekly gridded Aquarius L-band radiometer/scatterometer observations and salinity retrievals over the polar regions – Part 2: Initial product analysis, <i>The Cryosphere</i> , 8(3), 915-930, doi:10.5194/tc-8-915-2014.	
<b>RD30</b>	Olmedo, E., C. Gabarró, V. González-Gambau, J. Martínez, J. Ballabrera-Poy, A. Turiel, M. Portabella, S. Fournier, and T. Lee (2018), Seven Years of SMOS Sea Surface Salinity at High Latitudes: Variability in Arctic and Sub-Arctic Regions, <i>Remote Sensing</i> , 10(11), 1772	
<b>RD31</b>	Supply, A., J. Boutin, J.-L. Vergely, N. Kolodziejczyk, G. Reverdin, N. Reul, and A. Tarasenko (2020b), New insights into SMOS sea surface salinity retrievals in the Arctic Ocean, <i>Remote Sensing of Environment</i> , 249, 112027, doi:https://doi.org/10.1016/j.rse.2020.112027.	
<b>RD32</b>	Tang, W., S. Yueh, D. Yang, A. Fore, A. Hayashi, T. Lee, S. Fournier, and B. Holt (2018), The Potential and Challenges of Using Soil Moisture Active Passive (SMAP) Sea Surface Salinity to Monitor Arctic Ocean Freshwater Changes, <i>Remote Sensing</i> , 10(6), 869.	
<b>RD33</b>	Vazquez-Cuervo, J., C. Gentemann, W. Tang, D. Carroll, H. Zhang, D. Menemenlis, J. Gomez-Valdes, M. Bouali, and M. Steele (2021), Using Saildrones to Validate Arctic Sea-Surface Salinity from the SMAP Satellite and from Ocean Models, <i>Remote Sensing</i> , 13(5), 831.	
<b>RD34</b>	Tarasenko, A., A. Supply, N. Kusse-Tiuz, V. Ivanov, M. Makhotin, J. Tournadre, B. Chapron, J. Boutin, N. Kolodziejczyk, and G. Reverdin (2021), Properties of surface water masses in the Laptev and the East Siberian seas in summer 2018 from in situ and satellite data, <i>Ocean Sci.</i> , 17(1), 221-247, doi:10.5194/os-17-221-2021.	
<b>RD35</b>	Supply, A., J. Boutin, J.-L. Vergely, N. Martin, A. Hasson, G. Reverdin, C. Mallet, and N. Viltard (2018), Precipitation Estimates from SMOS Sea-Surface Salinity, <i>Quarterly Journal of the Royal Meteorological Society</i> , 144(S1), 103-119, doi:https://doi.org/10.1002/qj.3110.	
<b>RD36</b>	Supply, A., J. Boutin, G. Reverdin, J.-L. Vergely, and H. Bellenger (2020a), Variability of Satellite Sea Surface Salinity Under Rainfall, in <i>Satellite Precipitation Measurement: Volume 2</i> , edited by V. Levizzani, C. Kidd, D. B. Kirschbaum, C. D. Kummerow, K. Nakamura and F. J. Turk, pp. 1155-1176, Springer International Publishing, Cham, doi:10.1007/978-3-030-35798-6_34.	
<b>RD37</b>	Hasson, A., M. Puy, J. Boutin, E. Guilyardi, and R. Morrow (2018), Northward Pathway Across the Tropical North Pacific Ocean Revealed by Surface Salinity: How do El Niño Anomalies Reach Hawaii?, <i>Journal of Geophysical Research: Oceans</i> , 123(4), 2697-2715, doi:https://doi.org/10.1002/2017JC013423.	
<b>RD38</b>	Boutin, J., N. Martin, G. Reverdin, S. Morisset, X. Yin, L. Centurioni, and N. Reul (2014), Sea surface salinity under rain cells: SMOS satellite and in situ drifters observations, <i>Journal of Geophysical Research: Oceans</i> , 119(8), 5533-5545, doi:https://doi.org/10.1002/2014JC010070	

## 1.4 Acronyms

AD	Applicable Document
ATBD	Algorithm Theoretical Basis Document
Aquarius	NASA mission



*Climate Change Initiative+ (CCI+)*  
*Phase 1*  
Algorithm Development Plan

Ref.: ESA-CCI-PRGM-EOPS-SW-17-0032

Date: 14/09/2021

Version: v3.1

Page: 5 of 47

CCI	The ESA Climate Change Initiative (CCI) is formally known as the Global Monitoring for Essential Climate Variables (GMECV) element of the European Earth Watch programme
CCI+	Climate Change Initiative Extension (CCI+), is an extension of the CCI over the period 2017–2024
CMEMS	Copernicus Marine Environmental Monitoring Service
DARD	Data Access Requirements Document
DOI	Digital Object Identifier
DPM	Detailed Processing Model
ECMWF	European Centre for Medium Range Weather Forecasts
ECV	Essential Climate Variable
EO	Earth Observation
FOV	Field Of View
Hs	Significant Wave Height (see also SWH)
KS	Klein and Swift sea water dielectric constant model
MW	Meissner and Wentz sea water dielectric constant model
NASA	National Aeronautics and Space Administration
NOAA	National Oceanic and Atmospheric Administration
NOP	Numerical Ocean Prediction
NWP	Numerical Weather Prediction
OTT	Ocean Target Transform
SSS	Sea Surface Salinity
SST	Sea Surface Temperature
SWH	Significant Wave Height (see also Hs)
TBC	To Be Completed
UCR/CECR	Uncertainty Characterisation Report (formerly known as the Comprehensive Error Characterisation Report)
URD	User Requirements Document
VOS	Volunteer Observing ships
WS	Wind Speed



## 2 Plan for L-band data based CCI+SSS Algorithms

### 2.1 Input Level 2/Level 3 Data

In year 1, the input data to the CCI algorithms are levels 2 for SMOS and SMAP or Level 3 for Aquarius sensor. These data are all projected on the same EASE grid at a spatial sampling of 25 km. In year 1, the L2 products used for each sensor come directly from official space agency entrusted centres (e.g., CATDS, RSS). They are therefore not generated by the CCI processing chains and are the following for each sensor:

- **SMOS:** In year 1, we directly use as input for SMOS data the L2 products generated internally by the CATDS. These are the so-called L2P products based on SMOS ESA L2 v622 algorithm [AD.2, AD.3]. These products are provided onto an EASE grid at 25km resolution and are classified/filtered according to an ensemble of quality flags. The data are split into ascending and descending products. SSS is also classified according to the distance to the sub-satellite track.
- **SMAP:** In year 1, we directly use as input for SMAP sensor the RSS Level 2 v3.0 products. These are swath SSS from SMAP provided daily at 40 km resolution. The data are split into ascending and descending products and between the fore and aft views. Details on the processing algorithms can be found in [AD.6].
- **Aquarius:** we use as input the official release products L3 v5.0, which is the official end of mission public data release from the AQUARIUS/SAC-D mission (with DOI: 10.5067/AQR50-3SADS and which are accessible [here](#)). Aquarius Level 3 sea surface salinity (SSS) standard mapped image data contains gridded 1-degree spatial resolution SSS averaged over daily, 7 day, monthly, and seasonal time scales. We use the daily average dataset for generating the CCI-SSS L4 dataset of year 1. An average of ascending and descending products over the 3-radiometer footprint is performed. The ATBD for these Aquarius L3 products is detailed in [AD.4] and [AD.5].

### 2.2 Plan for L3 algorithms

L3 products are, by definition, time and space-averaged products obtained sensor by sensor, without mixing inter-sensor information. Here, we consider simple weighted averages of swath Level 2 SSS products, which may have been already corrected for some biases (e.g. land sea contamination or spatio-temporal drifts corrections in the brightness temperatures of the instrument such as the Ocean Target Transformation). These products can thus be used as a reference in terms of observed SSS variability since we don't apply to the observed SSS any specific smoothing operation (for example, by allowing introducing representativity errors or variance filtering).

A priori, these products will not be distributed to users except upon specific requests. They will be made available as part of the validation and verification of products and will serve to build up the Level 4 products.



### 2.2.1 Input Data re-gridding

While the SMOS Level 2 data are provided at CATDS onto the EASE grid at 25 km resolution, the SMAP Level 2 data and the Aquarius Level 3 products are not given on that grid. A first step will therefore consist in interpolating both the Aquarius and SMAP SSS onto the EASE grid at 25 km resolution. A bilinear interpolation scheme will be used for that purpose.

### 2.2.2 Space-time aggregation

The space-time aggregation of the input data will be calculated for each grid node and on a daily or decade temporal sliding window. Using an average weighted by the errors  $\sigma_t^2$  of each SSS product.

The monthly L3 products contain the averaged SSS field and the associated error for each L-band sensor: SMOS, Aquarius and SMAP.

## 2.3 Plan for L4 algorithms

### 2.3.1 Overview

The approach that will be adopted to generate Level 4 CCI+SSS products (which are distributed to the community) is as follows:

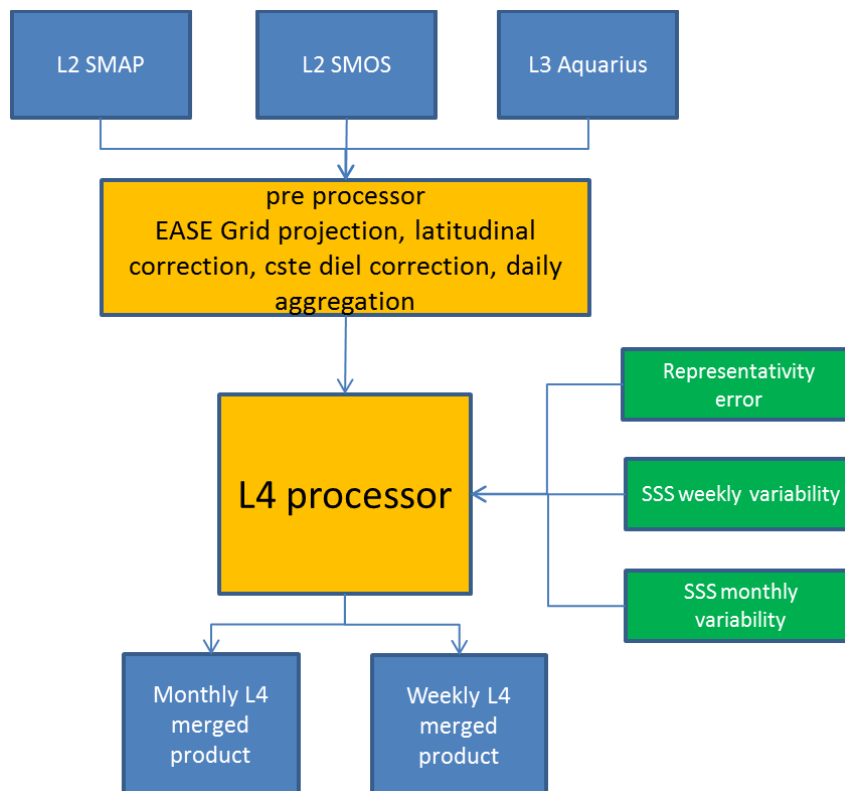


Figure 1: main L4 processing steps.

The first step will be to apply bias corrections to the input data. These exploit as much information as possible from the data themselves. SSS that seem to be affected by various



contaminations (coastal, RFI, galactic, solar, etc.) will be kept. There are sources of constant bias over time which vary as function of the location on the globe, the instrument and the geometry of observation and there are sources of bias that are not constant over time and depend on latitude. For these reasons, we plan to model the bias as a sum of two components:  $bc$ , the coastal bias and  $bl$  the latitudinal bias. We will consider that the latitudinal (orbital) biases are independent of the basin (Atlantic, Pacific or Indian Ocean) and that they apply in addition to the coastal/land biases.  $bc$  and  $bl$  can be estimated independently starting with the estimation of  $bl$  on open sea areas at grid nodes sufficiently far away from the coasts. Then, a latitudinal correction will be applied to the coastal pixels. From these latitudinal bias corrected data, we shall estimate  $bc$ . Since the number of independent subsets of data is relatively large, the different biases can be estimated in a self-referenced way, i.e. there is no need for an external reference when considering SSS anomalies rather than absolute salinities. The L4 products, represented by  $SSS(t)$  are therefore estimated together with the biases in each product. The error propagation occurs at the time of this estimate using a Bayesian least square method that includes a time correlation length. We plan to process each grid node independently of each other and thus maintain the native spatial resolution of each sensor.

The self-consistency of the measurements (averaged in a monthly time window) over the whole time period (several years), and taking into account the natural variability of the SSS expected in this window, will allow the different inter-sensor biases to be corrected relatively to each other. A posteriori 3 sigma filters will then be applied to remove outliers. These filters will be applied with respect to the natural SSS variability that must be taken into account in the satellite SSS estimation process. Indeed, if a low variability is expected, the filters applied must be more severe. Otherwise (e.g., at river mouths or in strong currents where variability is high), data that differ significantly from the mean should be retained.

The self-consistency criteria considered in the algorithms will be temporal. A spatial correction of the SSS according to a certain reference (e.g. WOA climatology) could affect spatial and temporal dynamics and could remove some of the interannual signals and mesoscale signatures. We will therefore consider coastal/ocean biases that are constant over time. These biases can be corrected without affecting geophysical SSS dynamics. In practice, the SSS correction/estimation is done grid node per grid node considering the inter-sensor self-consistency in SSS. To correct seasonal latitudinal biases, a relative correction will be finally applied. It applies to all basins and should not affect the interannual dynamics.

The different corrections are relative. As a result, SSS anomalies are available at the end of the correction processing. These anomalies are then calibrated against an absolute reference. Ideally, this shift should be a time-independent correction in order to maintain the temporal dynamics of the SSS. In some cases (e. g. high latitudes), coastal biases are not constant over time due to variations in ice edges. A specific processing shall be found in these areas and will be the subject of future studies.

In the settings of the various processing parameters, either spatially smooth fields or slowly evolving time fluctuations will be estimated to reduce errors as much as possible. This is why the CCI+SSS L4 products will be split into two sub-products: a monthly product and a weekly product.



The L4 products will therefore be estimated together with the biases in each product. The error propagation occurs at the time of this estimate using a Bayesian least square method that includes a time correlation length. We will process each grid node independently of each other and thus maintain the native spatial resolution of each sensor.

### 2.3.2 Detailed plan for the level 4 algorithm steps

The Level 4 algorithm steps to perform the corrections in order to estimate the unbiased SSS will be as follows:

1. Correction of the **bias related to the modelling of the L-band sea water dielectric constant at low SST**. L2 and/or L3 data will be first filtered to discard outliers. In the case of SMOS, an empirical correction of the retrieved SSS at low SST will be applied to correct for Klein and Swift (KS) dielectric constant model biases at low temperatures (Zhou et al. 2017). A filter is also applied to remove data which exhibit a cost-function retrieval Chi-parameter (given by the L2 products) which is strictly less than 3. The SST-correction related to the dielectric constant will be empirically derived from the differences observed with in situ data as a function of SST.
2. Correction of the **latitudinal biases** if necessary. Latitudinal bias is low for SMAP and Aquarius data that are already latitudinally adjusted via ARGO in-situ data. For SMOS data, a seasonal correction will be applied that depends on the latitude to ensure best consistency between SMOS, SMAP and Aquarius data. The latitudinal seasonal correction applied to the SMOS data will depend on the across track location and the orbit pass direction (ascending or descending). The purpose is to estimate the term  $bl$ , determined separately for ascending and descending orbits, on a monthly basis, and assumed to be independent of the longitude and of the year. We will neglect interannual variations that could result from variation in sun activity, as they appear to be an order of magnitude smaller than the seasonal biases. The correction shall be estimated from Atlantic Ocean orbits further than 800 km from continental coasts, in order to avoid land-sea contamination and because it is possible to reach very high latitude in comparison with Pacific Ocean.
3. Estimation of the **inter-sensor biases** and monthly SSS. At this stage and after SMOS latitudinal correction, it is considered that there are still possible **coastal biases** affecting the SMOS-SMAP-Aquarius data. These biases are considered constant over time and specific to each type of acquisition (term  $bc$ ). The types of acquisition include: the orbit direction (ascending/descending), except for the L3 Aquarius) and the geometry of acquisition (across-track location for SMOS and fore/aft viewing direction for SMAP). The correction of relative biases will assume that sensors observe the same SSS on average over a 2010-2018. The inter-sensor biases will be considered constant for each month and evaluated assuming SSS varies slowly over a month. This computation will be carried out by an optimal interpolation.
4. **Estimation of errors** of the monthly SSS. In the optimal interpolation, we shall consider that the SSS field has some monthly variability. This variability will actually be an RMSD estimated from an independent SSS global average on each grid node. The variability will be seasonal and the SSS will be allowed to fluctuate more or less around its mean value



with the seasons. In order to obtain monthly variability at all points and all seasons, we shall use SMOS filtered SSS fields for low latitudes and ISAS SSS fields [RD08] at the highest latitudes or at some points on the globe where RFI contamination is intermittent. This variability will be increased in order to always leave the possibility of unexpected fluctuations. In principle, when averaging data from different sensors, it makes sense if the acquisitions have the same spatial and temporal resolution. The temporal resolution of the Aquarius product we will use (7days) is much longer than the temporal resolution of SMOS and SMAP L2 SSS (on the order of 3 days) so that a representativity error corresponding to the SSS variability within 7 days should be taken into account. However, this representativity error remains low, partly because most SSS structures at 150km resolution do not vary much within 7days, compared to SMOS and SMAP measurement errors (representativity errors are quadratically added to measurement errors). The spatial resolution of Aquarius SSS is 150km, 50km for SMOS and SMAP, hence we must take into account a representativity error for Aquarius, corresponding to the variance of the SSS between 50 and 150km<sup>2</sup>. The aim is to increase the error associated with the Aquarius data by a representativity error that can be calculated from an ocean circulation model SSS such as Mercator. This information, calculated off-line, will be used in the cost function. Note that this representativity error will depend on the season and dynamics of the SSS field. Representativity errors are generally low in the open sea (compared to measurement errors) except in some areas of high gradients and in rainy areas. Close to the coast and at the river's mouths, these errors are difficult to assess because of the high interannual variability that puts the statistical approach into default. The algorithm will take into account Aquarius representativity errors due to the difference in spatial resolution and the low relative amplitude of Aquarius errors.

5. In order to **estimate the monthly SSS**, we will proceed in 3 steps:
  - 1) -a first estimation of the biases and time series of SSS, grid node by grid node will be performed,
  - 2)-a 3 sigma filtering of the observed SSS in comparison with the estimated SSS will be done. The aim here is to identify any outliers against the returned SSS field. Outliers can be linked to intermittent RFIs. It is considered here that stable RFI contamination can be corrected.
  - 3)-a second estimate of SSS biases and time series after removing outliers.

The relative biases used to derive monthly SSS will be estimated taking the averaged SSS from the SMOS central across swath location as a priori.

6. Correction of individual SSS and **computation of a weekly-averaged SSS field**. In this step, the bias correction will be fixed and the 30-day SSS field will be used as an a priori. We will estimate fluctuations around this monthly field to achieve a time resolution of 7 days. This computation will be carried out by an optimal interpolation. To estimate the weekly



SSS, the biases calculated at the monthly SSS are frozen (it is assumed that the biases will not be better estimated from a weekly smoothing). We will start from the monthly SSS as a priori. We will try to estimate the weekly fluctuations around this a priori. First, a 3-sigma filter will be used. Here,  $\sigma = \sqrt{\text{error\_L2OS}^2 + \text{variability}^2}$ . The variability will be given by Mercator model. This shall eliminate outliers that deviate too far from what is expected.

7. Estimation of **errors of the weekly SSS**. The computation of theoretical errors will be obtained directly from the pseudo hessian matrix (square matrix of second-order partial derivatives) used in the Optimal interpolation algorithm.

8. **Absolute calibration of salinities.**

At the end of the inter-sensor bias correction step, the salinities obtained are set on average on those of the SMOS ascending central dwell (or on the average of the SSS of all sensors if the central dwell is not observed). The central dwell can itself be affected by a bias that must be corrected by using the global average of the ISAS data over the period considered (thus, the dynamics of the SSS SMOS are not affected: only one constant value, grid node per grid node, is added for the entire period covering 2010-2018). This step will use the median or the quantile of the SMOS and ISAS time series. The value of quantile will depend on the SSS variability itself. The correction will allow matching the SMOS quantile and the ISAS quantile on the 30-day average data. We propose to perform the calibration of SMOS on ISAS, not by using the median but a high quantile (80%), in order to promote the calibration on the strong values of the SSS.

### 2.3.3 L4 products content

We plan to include the following fields in the L4 products:

-monthly and weekly SSS fields: obtained from OI algo

-SSS error: obtained from OI algo

-SSS mean bias: mean of the biases applied over the considered time interval (+/-30 days for monthly data and +/-10 days for weekly data).

-SSS std bias: mean of the biases applied over the considered time interval (+/-30 days for monthly data and +/-10 days for weekly data).

-number of outliers over the considered time interval (+/-30 days for monthly data and +/-10 days for weekly data).

-number of data over the considered time interval (+/-30 days for monthly data and +/-10 days for weekly data).

-quality flag =0 if no data present over the considered time interval (+/-30 days for monthly data and +/-10 days for weekly data).

-pct\_var :  $100 \times (\text{SSS error})^2 / \text{variability}$  (%)



These values will be given for each grid node and sampled every two weeks for monthly products and every day for weekly products.

## 2.4 Plan for the evolution of the L-band CCI algorithms for year 2

In year 2, we plan to prepare the second products and start to prepare the third Climate Research Data Package (CRDP):

### 2.4.1 2<sup>nd</sup> CRDP:

**The 2<sup>nd</sup> CRDP will cover the 2010-2019 period. It will be produced at the beginning of 2020.**

**L4 fields will be obtained from existing L3 Aquarius ,L2 SMAP and L2 SMOS** (Aquarius RSS v5, SMAP RSS v4, SMOS CATDS) with the following evolutions in the debiasing method (in order to solve the caveats identified in CRDP 1 (in blue below) or at least part of them) :

#### Evolution of the debiasing methodology

The SSS random error in the weekly product is overestimated by a factor  $\sim 1.4$ : the error model for weekly products will therefore be revisited

The Number of outliers is wrongly set to 'NaN' in the case where it is equal to zero and this will be corrected.

Products have not yet been optimized for some issues encountered at high latitudes (i.e. remaining ice, RFI pollution, biases due to land-sea contamination and dielectric constant in cold waters). To solve these issues, in CRDP 2 we plan the following changes:

- 1) The SST correction will be adapted from Dinnat et al. 2019 (see Figure 2, instead of Zhou et al. 2017 which included an SST dependency coming from a poor atmospheric model : SST correction will be approximately divided by a factor 2).
- 2) The wind speeds limited to below 16 m/s
- 3) Sea ice and RFI sorting will be refined using the retrieved SMOS ACARD parameter
- 4) We shall improve the absolute bias adjustment of the whole satellite time series relative to ISAS by adjusting, not only one quantile of SSS distribution, but by adjusting several quantiles of satellite SSS relative to ISAS SSS distribution quantiles
- 5) We'll use SMAP RSS v4 instead of SMAP RSS v3. In this product version 4, ice sorting is less severe in the Arctic ocean and shall provide more retrievals
- 6) the reference period to estimate systematic errors will start in 2013 (instead of earlier) in order to decrease the impact of RFIs in the northern Atlantic Ocean up to 2012 ( N.B. we'll need to check that this does not lead to degradations in other regions affected by RFIs in mid/end SMOS period (e.g. La Reunion or Japan RFI affected regions)



- The criteria for flagging data close to land (including islands) are conservative and likely to be too restrictive in places. Land mask is going to be revisited and a non-exclusive criterion will be used when merging SMOS and SMAP SSS

- There is a systematic global underestimation (-0.08) of SSS starting at the beginning of the data set, and gradually disappearing at the end of 2010. We will investigate the possibility of putting a linear time correction in 2010, but the region where it must be applied needs to be well defined (the trend is not visible in the Southern Ocean for example)

- There is a seasonal varying bias (~0.1, peaking in the middle of the year) in the Pacific North of 25°N». SST and wind speed thresholds may help to decrease this bias

**In addition to L4 products we will generate debiased L2 and L3 (TBD). The 10-year processing will be run onto AdwaisEo machines.**

**CDRP 2 is planned to be delivered to the validation group in April 2020 in order to get feedbacks before the annual review.**

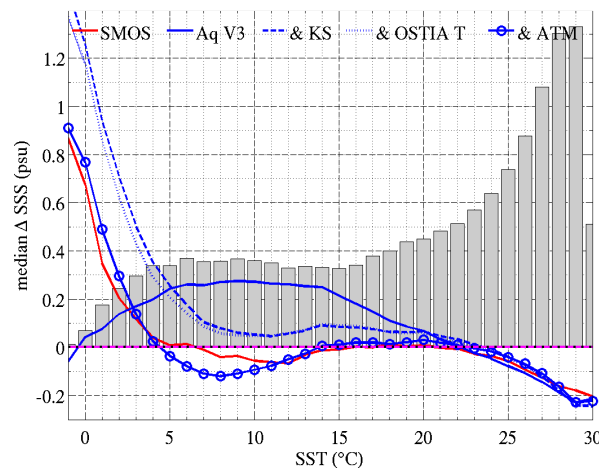


Figure 2 SST dependence of SSS bias for (red) SMOS and (blue) Aquarius. Bias is computed as differences between satellite SSS and Argo in situ measurements over the Aquarius era (Dinnat et al., 2019, RD15).

#### 2.4.2 3rd CRDP (2020-2021 period)

**L2 SMOS SSS will be reprocessed by the CCI team with another configuration than the one used by the SMOS operational chain in order to study/correct the influence of the dielectric constant model and of the errors on ECMWF SST in post processing**

- L2 SMOS will be regenerated using SMOS L1v6 Tb with the following configuration (ECMWF auxiliary parameters will be kept as priors):

- SSS1 without SST retrieval (Klein and Swift dielectric constant model)
- SSS2 without SST retrieval (new dielectric constant model, BV, under validation)
- ACARD with SST retrieval, new dielectric constant model, BV



We will start by a one year retrieval on the global EASE grid (processing time : 2 days for processing 3 months of SMOS data on 12 computer nodes) – Once this processing will have been carefully checked a complete processing on the EASE global grid and on the EASE arctic grid will be launched

- 1) L3 maps will be generated allowing to thoroughly evaluate the impact of the model change and of erroneous SSTs
- 2) Effects of auxiliary field changes will be estimated using the Jacobians  $dT_b/dSSS$ ,  $dT_b/dSST$  (possibly  $dT_b/dWS$  if time permits). We will then investigate the relevance of changing the SST prior field, e.g. changing OSTIA SST to the CMC SST (used in SMAP and AQUARIUS processing, Meissner et al. 2016);
- 3) -Analyse the effect of changing the dielectric constant parametrisation using at least one year of data
- 4) Depending on the above analysis, we will include a SST correction in SMOS SSS debiasing and/or in SMAP and AQUARIUS SSS processing as a function of SST differences

**We will generate L4, L3 and L2 debiased products. To be delivered to the validation team during the first part of 2021.**

## **2.5 Plan for the evolution of the L-band CCI algorithms for year 3**

As announced in 2.4, the L-Band CRDP version 3, contrary to the version1 and version2, will be built using SMOS Level 2 SSS processed by the CCI project itself.

Thanks to a collaboration with the Aquarius team (E. Dinnat, NASA) and with the SMOS/ESA Expert Support Laboratory (ESL) team, we have developed and validated a new dielectric constant parametrization that will be used in the SMOS-CCI L2 v3 processing. A paper describing this new model is in revision (Boutin et al. IEEE TGRS). It is this new parametrization that will be used in SMOS-CCI version 3, instead of a SST-bias correction (Figure 2).

The SMOS-CCI L2 v3 will also use a modified Ocean Target Transformation (OTT) processing. The OTT is a vicarious calibration of SMOS  $T_b$  estimated in the south-east Pacific region. In the operational SMOS processing it is estimated using the World Ocean Atlas (WOA) SSS climatology. In the SMOS-CCI L2 v3 processing, WOA SSS will be replaced by monthly ISAS SSS fields, as we observe small but non-completely negligible interannual variability between both fields in that region (leading to typically .02K systematic error in  $T_b$ , ie typically 0.1pss in cold regions).

Another change concerns the SST retrieval made in the SMOS operational processing. It will be removed in the SMOS-CCI L2 v3, thus enabling an a posteriori correction for differences between ECMWF SST (used in SMOS processing) and Canadian Meteorological Center (CMC) SST (used in SMAP and Aquarius processings). We do not exclude a possible adjustment to another reference SST than ECMWF or CMC SST, if we identify a more precise reference product providing a measure of subskin temperature (at 1cm depth). This is especially critical for cold waters (the location where L-band SSS retrieval is most sensitive to a SST error).





CCI products are projected on a EASE grid. CCI version 1 and version 2 use the rectangular EASE grid. Version 3 CCI products will be delivered on both rectangular and polar EASE grids. Concerning grid points in the vicinity to land, CCI version 1 and 2 used a nearest neighbor criteria to collocate ISEA (the grid used by the SMOS level 2 processor) and EASE (the CCI grid) grid points which may lead to artificial land contamination. This criterion will be revised in order not to select grid points of the ISEA grid too close to land in the CRDP version 3.

During the SMOS commissioning phase (Jan-June 2010), SMOS measurements have been acquired alternatively in Full polarization and Dual polarization modes. There were always in FP afterwoods. CCI version 1 and 2 only use FP Tb. An attempt will be made in CCI version 3 to add SMOS SSS retrieved in DP mode.

SMOS-CCI L2 v3 will be regenerated using SMOS L1v6 Tb with the following configuration (ECMWF auxiliary parameters will be kept as priors):

- SSS1 without SST retrieval (OTT1 computed with ISAS)
- SSS2 without SST retrieval (OTT2 computed with WOA)
- ACARD with SST retrieval (OTT1 computed with ISAS)

One year processing will be launched in Summer 2020 to test these configuration changes.

The SST adjustment processing will be studied in LOCEAN in Summer 2020 and a correction/adjustment prototype delivered to ACRI/Adwiseo in Fall 2020.

Le level 3 and level 4 processings will be updated as far as feasible to comply with validation and climate user teams feedbacks.

The full 2010-2020 reprocessing will be made available to validation team and climate users before April 2021.

## **2.6 Plan for the evolution of the L-band CCI algorithms for phase 2**

In phase 1, SSS measurements from the three L-band satellite sensors have been merged to produce CCI L4 SSS time series over a decade at global scale. The methodology we have developed for building the CCI L4 dataset aims at preserving the SSS variability globally observed by satellite every few days in footprints integrated over typically 50 x 50 km<sup>2</sup>. No spatial smoothing nor temporal relaxation to in-situ SSS have been introduced in order to keep as much as possible SSS interannual variability sensed by original SSS satellite measurements. On another hand, the self-consistency between satellite SSS measured by the various sensors and under various geometries have been used to correct for systematic uncertainties. External SSS information is considered only for calibrating the long term SSS absolute value and for estimating representativity uncertainties. The CCI+SSS approach is, therefore, upstream of the optimal interpolations which correct satellite SSS biases using in-situ SSS fields on a monthly basis or less, such as (Melnichenko et al., 2016), and the CCI+SSS fields could be used as inputs to such method,



as was done with SMOS data (Nardelli et al., 2016) or with SMOS and SMAP data (Kolodziejczyk et al., 2020).

Nevertheless, some issues have been identified in the PVASR which remain to be tackled in future versions:

- in the high northern latitudes, both seasonal latitudinal biases and land-sea contamination (and/or ice-sea) contamination affect all SMOS ocean pixels. Hence a method which separates the determination of the two (or three) types of contamination does not allow to remove all the contaminations. The methodology should be adapted to deal with both contaminations.

-The interannual variation of SMOS SSS biases after systematic bias correction has not been fully removed with the use of ISAS for OTT computation and the use of ERA5 auxiliary parameters. The recent release of SMOS L1/L2 v7, now operated operationally, is subject to different biases but still with an interannual variability. To which extent, the methods used with SMOS v6 could be successfully applied to SMOS v7 should be explored. One issue is whether the full SMOS FOV should be considered or only part of it (eg AFFOV) without losing too much SSS precision. The ice contamination with SMOS v7, stronger than with v6, especially on ascending orbits in the Southern hemisphere should also be considered with great care.

-The ERA5 auxiliary parameters have been used instead of ECMWF forecasts without changing the direct models. The consequence of this choice should be further evaluated.

-Although smaller than the SMOS seasonal latitudinal biases, the Aquarius seasonal and latitudinal biases have been found to play a major role in biases before 2015. Hence they should be corrected before these data are ingested in CCI L4.

-A new version of SMAP (RSS v5) is foreseen to be released in Fall 2021. Together with SSS, it will provide SSS uncertainties which could be interesting to introduce in CCI processing.



## 3 Plan for C and X-band data based CCI SSS algorithm

### 3.1 Short overview of the physical principle of SSS retrieval from C- and X-band radiometer data

---

The potential SSS retrieval capability from low frequency spaceborne radiometer data operated at C (6.9 GHz) and X (10.7 GHz) band beyond several other frequencies (AMSR-E, AMSR-2, WindSAT, or, HY-2A) has been demonstrated in RD09 for the very high SSS gradients and warm Amazon river Plume area. This principle was more recently applied to the SSS signal in the China Sea by RD10 using the same frequency channels data from the microwave radiometer onboard the HY-2A satellite.

Though the response of sea surface reflectance to surface salinity is relatively weak in the C- and X- band compared with L-band used on the SMOS, Aquarius-SAC/D or SMAP satellite missions (see ), the SSS signal is significantly improved after differentiating the sea surface reflectance between the C and X band. We explain this further below.

The objective of the AMSR, AMSR-E, AMSR-2, WindSat or HY-2A microwave radiometers is to acquire global observations of the sea surface temperature, wind speed, water vapor and cloud liquid water. These instruments are (in general) equipped with twelve channel, six-frequency, passive microwave radiometer system. They measure horizontally and vertically polarized brightness temperatures at 6.9 GHz, 10.7 GHz, 18.7 GHz, 23.8 GHz, 36.5 GHz, and 89.0 GHz and with incidence angle  $\sim 53-55^\circ$ . Note that AMSR-2 has 2 additional frequency channels at 7.3 GHz used for RFI detection.

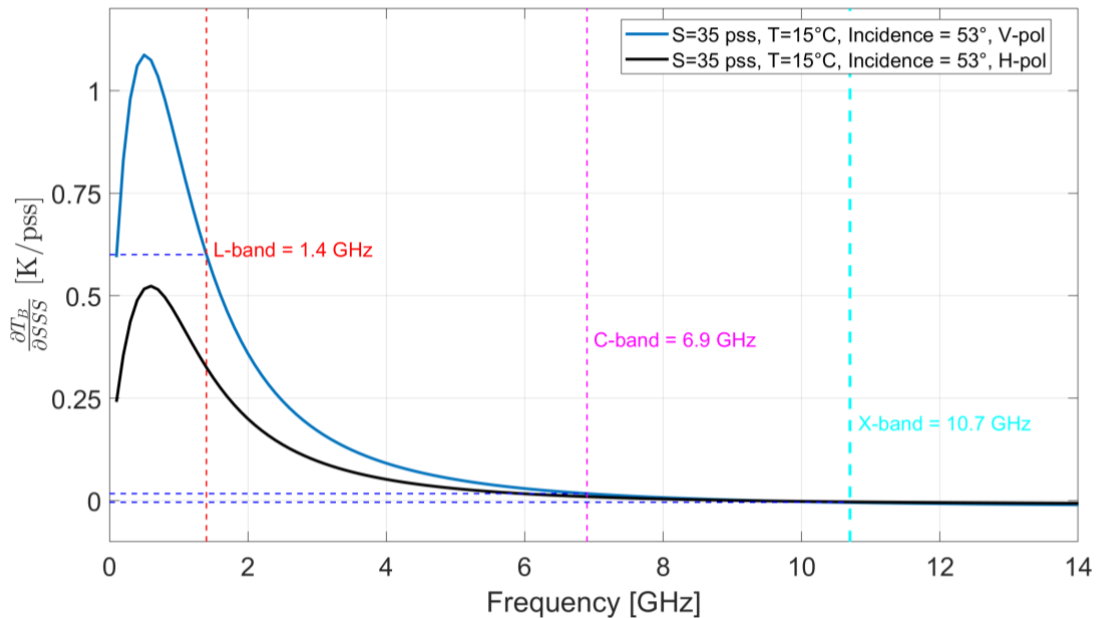


Figure 3 Sensitivity of the flat ocean brightness temperature to SSS, namely,  $\frac{\partial T_B}{\partial SSS}$  as a function of electromagnetic frequency (x-axis) computed from Klein and Swift (1977) for the salinity of 35 psu and temperature of 15°C with a fixed incident angle of 53°.

As shown in Figure 3, the response of the sea surface reflectance to sea surface salinity is sensitive near 1.4 GHz and drops sharply as microwave frequency increases for a given SST for both horizontal and vertical polarizations (H-pol and V-pol), while the signal is stronger for the V-pol. At 53° of incidence, SST=15°, SSS=35 pss, and V-polarization, the sensitivity thus drops from ~0.6 K/psu at L-band to ~0.02 K/psu at C-band and the brightness is almost insensitive to SSS at X-band.

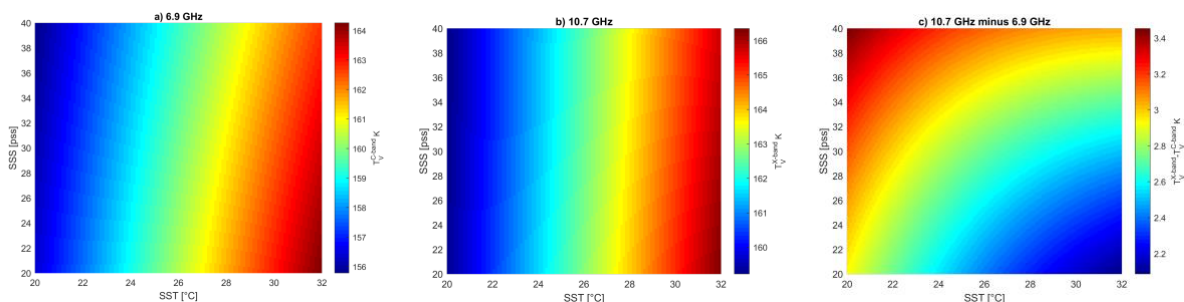


Figure 4 Brightness temperature of sea surface in microwave bands as functions of SSS and SST. (a) brightness at 6.9 GHz (C band) (b) Brightness at 10.7 GHz (X band) in V-pol and (c) brightness temperature difference between the 10.7 GHz and 6.6 GHz in V-pol.

To evidence nonetheless the capability of C/X band radiometer channels for measuring the sea surface salinity, the brightness temperature of the sea surface in microwave bands is computed as functions of SSS and SST (Figure 4) following Klein and Swift (1977)'s model for the dielectric constant of sea water. For a given SST, the flat ocean surface  $T_b$  in V-polarisation decreases monotonically with increasing SSS, while the reflectance of sea surface increases due to the

presence of saline materials that increase the dielectric properties of sea water and thus decrease the emissivity or increase the reflectance. Meanwhile, for a given SSS, the surface emissivity (reflectance) increases (decreases) due to higher molecular energy with higher temperature (Figures 3a and 3b). By differentiating the reflectance between the C and X band in vertical polarisation, it is clearly seen in Figure 3c that both SSS and SST have apparent impacts on the differential X- minus C-band reflectance of sea surface, which is defined as:

$$\Delta R = R_{10.7V} - R_{6.6V}$$

Given an auxiliary information on the SST, SSS can then be derived from  $\Delta R$  using the model shown in c. An accurate estimation of the ‘flat’ surface brightness frequency-differential contrast  $\Delta R$  quantity is therefore a key step of the proposed algorithm.

### 3.2 Algorithm Development plan

From a complete data processing perspective, the SSS retrieval procedure in the context of the CCI-SSS project from the C/X band radiometer satellite includes data pre-processing from swath brightness temperature data (so-called Level 1A) of the scanning radiometer of AMSR-E or AMSR-2 satellite to brightness temperature TAB at antenna level. The Level 2B geophysical products (SST, surface wind speed, cloud liquid water, and columnar water vapor) available from dedicated centers (JAXA, NSIDC) will also be gathered with the brightness temperature TAB.

AMSR-E/2 swath data flagged for rain, low sun glint angles and low Geostationary Radio Frequency Interference (RFI) angles will be first discarded. The vertically polarized L1A TB products (antenna level) at each AMSR-E/2 frequency  $f$ , hereafter denoted  $\tilde{T}_v^f$ , can be expressed as:

$$\tilde{T}_v^f = T_{up}^f + \tau^f [e_v^f T_s + r_v^f (\tilde{\Omega}_v^f T_{down}^f + \tau^f T_c)] \quad (1)$$

where  $e_v^f$  is the sea surface emissivity in v-polarization and the corresponding reflectivity is  $r_v^f = 1 - e_v^f$ .  $T_{up}^f$  is the upwelling atmospheric brightness temperature at the top of the atmosphere,  $T_{down}^f$  is the downwelling atmospheric brightness temperature at the surface,  $\tau^f$  is the atmospheric transmissivity and  $T_s$  is the SST.  $T_c \sim 2.7$  K is the cosmic background radiation temperature. The  $\tilde{\Omega}_v^f$  term is a correction factor to account for nonspecular reflection of the atmospheric downwelling radiation from the rough surface towards the radiometer. Given the AMSR-E/2 Level2B water vapour, cloud liquid water and surface wind speed products, as well as the co-localized external SST products (TDB: CCI SST, or GHRSSST SST products),  $T_{up}^f$ ,  $T_{down}^f$ ,  $\tau^f$  and  $\tilde{\Omega}_v^f$  can be evaluated using the algorithm described by RD.11 and evolutions presented in RD.12 and RD.13. The surface reflectivity in v-pol at frequency  $f$  can then be estimated using equation (1) as:

$$r_v^f = \frac{\tilde{T}_v^f - T_{up}^f - \tau^f T_s}{\tau^f [\tilde{\Omega}_v^f T_{down}^f + \tau^f T_c - T_s]} \quad (2)$$

Using , the difference  $\Delta T_b^v$  in brightness temperature estimated at the surface level between 6.9 GHz ( $T_v^{6.9}$ ) and 10.7 GHz ( $T_v^{10.7}$ ) vertical polarization channels is

$$\Delta T_v^f = T_v^{6.9} - T_v^{10.7} = T_s(r_v^{10.7} - r_v^{6.9}) \quad (3)$$

where  $\Delta T_v^f$  includes the sum of two contributions:

$$\Delta T_v^f = \Delta T_v^{flat} + \Delta T_v^{rough}$$

The first one,  $\Delta T_v^{flat}$ , is the difference in the flat surface ocean reflectivity between the two channels ( $\Delta r_{flat}$ ) and the second one,  $\Delta T_v^{rough}$ , is due to a possibly differing surface roughness impact on the reflectivity ( $\Delta r_{rough}$ ) at the two frequencies [RD.14].

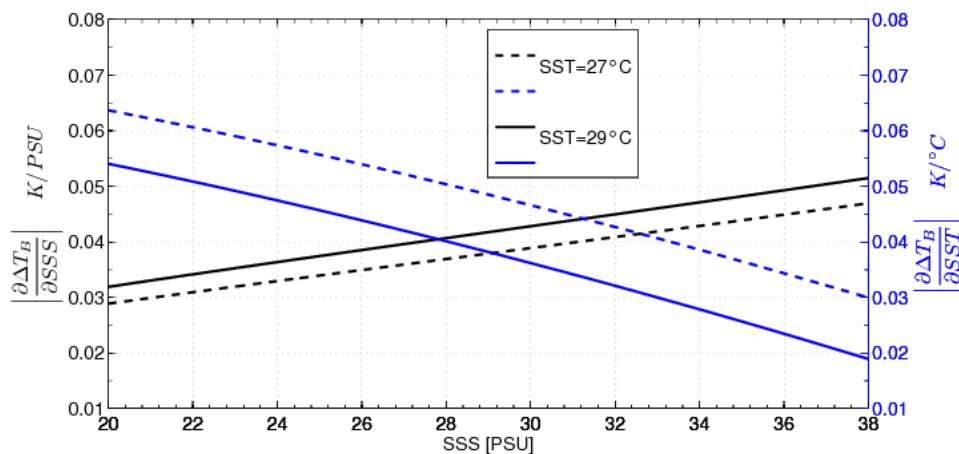


Figure 5 Sensitivity of  $\Delta T_B = T_{B6.9V} - T_{B10.7V}$  to SSS & SST

As shown in Figure 5, the flat ocean contribution to  $\Delta T_B$  is more sensitive to SSS than SST for  $SSS > 28$  at  $SST = 29^\circ C$  and for  $SSS > 33$  at  $SST = 27^\circ C$ . At  $SST = 29^\circ C$  &  $SSS = 35$  pss,  $\frac{\partial \Delta T_B}{\partial SSS} \cong -0.05$  K/psu &  $\frac{\partial \Delta T_B}{\partial SST} = 0.025$  K/°C, so the use of the frequency-differential quantity  $\Delta T_B$  strongly minimizes the SST impact on the signal but the latter still need to be corrected for, and accurate external SST data are needed for the SSS retrieval algorithm.

The second contribution come from differing surface roughness impact on the reflectivity ( $\Delta r_{rough}$ ) at the two frequencies. As found in a preliminary analysis (one global month of data from AMSR-E) and shown in Figure 6, the evolution of brightness temperature in V-polarization with surface wind speed is very similar in the two frequencies and the difference is almost wind-speed independent in the range of wind speed from 4 to 10 m/s.

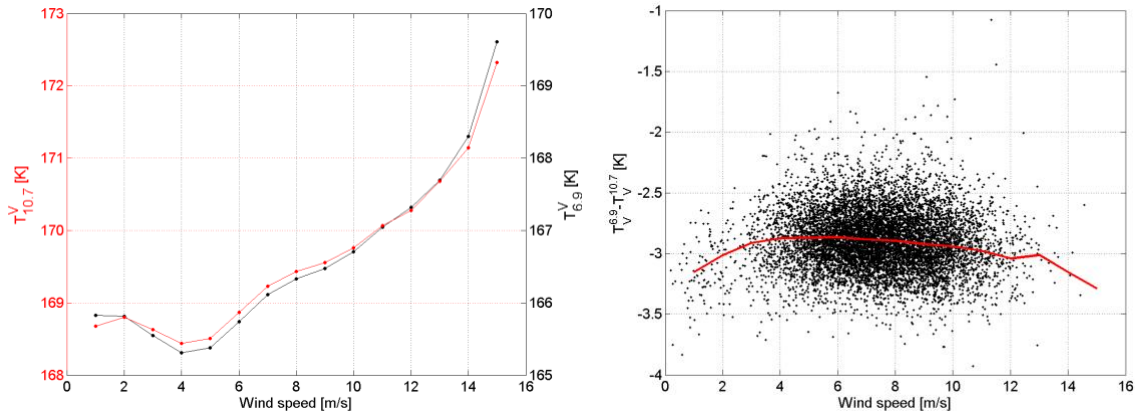


Figure 6 Surface brightness temperature evolution as a function of surface wind speed for X-band channel in V-pol (red) and C-band channel in V-pol (black)

As a first assumption, SSS will only be retrieved in these moderate wind speed conditions and we will assume similar sensitivity to wind speed in the two frequencies so that  $\Delta T_v^{rough} \sim 0$ .

A common database of AMSR-E and/or AMSR-2  $\Delta T_B$  and the CCI-SSS products v1.8 will be collected over four specific regions of warm tropical regions with high SSS gradients:

- Region 1: Mississippi river plume [98°W- 81°W;24°N-31°N]
- Region2: Amazon & Orinoco river plumes [78°W-25°W;5°N-30°N]
- Region 3: Congo river plume: [0°-13°E; 10°S- 0°S]
- Region 4: Bay of Bengal [79°E-98°E;9°N 22°N]

Part of the database (covering 2010-2018) will be used to train and adjust empirically the algorithm, assuming the CCI-SSS product is the ground truth. This step is needed to adjust for residual errors in the RTM corrections to estimate  $\Delta T_B$ . Using the external SST product and the CCI-SSS, the modelled  $\Delta T_B^{KS}$  can be estimated using Klein and Swift dielectric constant model and be compared to the AMSR-E ( $\Delta T_{B}^{AMSR-E}$ ) or AMSR-2 ( $\Delta T_{B}^{AMSR-2}$ ) estimated brightness temperature contrasts.



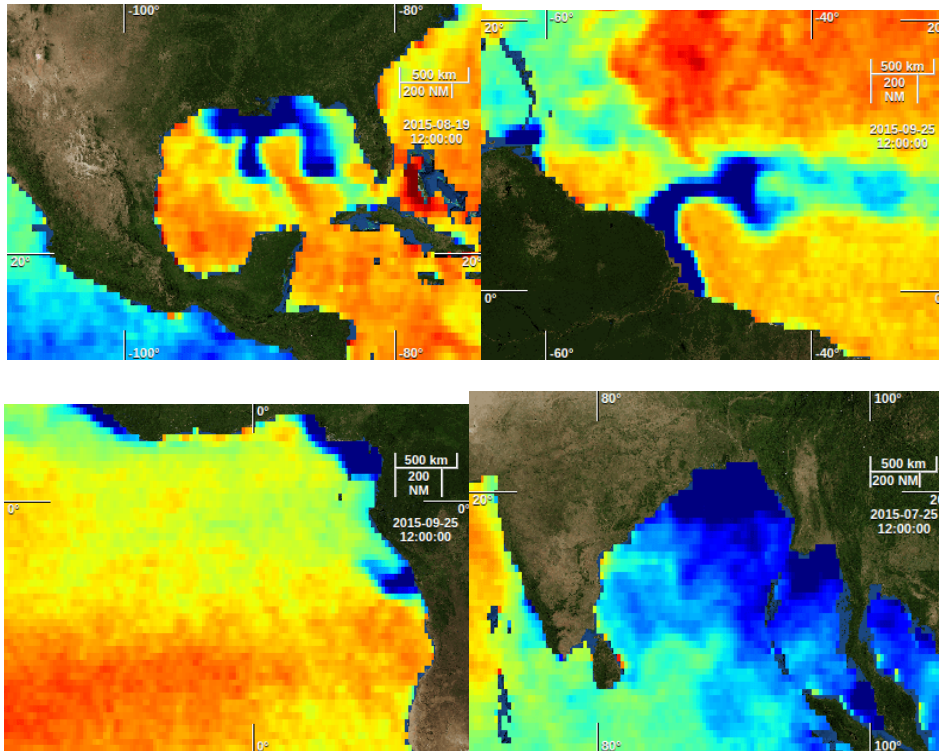


Figure 7 Oceanic Regions where SSS data shall be analyzed and produced using C/X band radiometer data

By using an external auxiliary SST product and SSS from the first CCI SSS data based on L-band products alone, the modelled brightness  $\Delta T_{B_{KS}}$  will be computed with the KS model at C and X band.

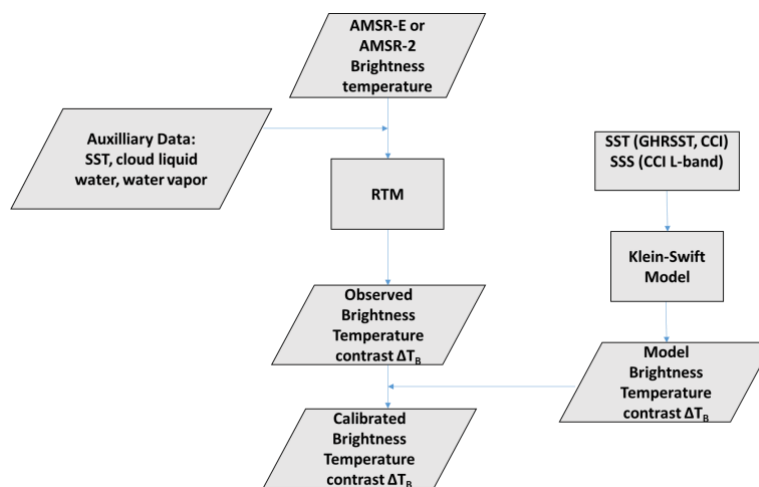


Figure 8 Brightness temperature calibration procedure for the SSS retrieval from AMSR-E or AMSR-2 radiometer data. The auxiliary data include SST, wind speed, cloud, liquid water, and water vapor used in the RTM. In KS model, SST is from GHRSSST and SSS from the CCI v1.8 dataset.





The  $\Delta T_B^{\text{AMSRE}}$  observed by the AMSR-E (or AMSR-2) satellite will then be calibrated with the modelled  $\Delta T_B^{\text{KS}}$  for the next step of SSS retrieval (Figure 8). The calibration procedure will consist of two steps:

Firstly, the matchups for  $\Delta T_B^{\text{AMSRE}}$  and  $\Delta T_B^{\text{KS}}$  will be selected and the calibration coefficients for  $\Delta T_B^{\text{AMSRE}}$  will be computed through a least-square fit or other empirical correction methods for each month of a full year and each region. Note that the exact method for empirical adjustments of the calibration are still to be determined: multi-variable linear regression or neural network, or others. The calibration coefficients for each month shall be statistically stable and do not change much with time and hopefully from one region to the next but we anticipate regional differences in the RTM inaccuracies.

Secondly, the SSS products will then be retrieved by using the calibrated  $\Delta T_B^{\text{AMSRE}}$  between C and X bands of the AMSR-E and AMSR-2 radiometers using a (or several) look up table(s). An estimation of the error propagation will be provided taking into account the radiometric accuracy, RTM model and auxiliary data information.

The C-band retrieved SSS shall be gridded with 0.25-degree latitude by 0.25-degree longitude on a monthly scale. We expect to back-up SSS from each sensor in time to cover periods as follows:

- AMSR-E on NASA's EOS Aqua spacecraft launched May 4, 2002. The instrument stopped rotating Oct 4, 2011.
- AMSR-2 on JAXA's GCOM-W1 spacecraft, launched May 18, 2012. This instrument is currently operating.

Using AMSR-E data, one shall therefore be able to reconstruct SSS over each selected region since mid-2002.

The plan is to deliver first C/X-band CCI-SSS data in between mid and end 2020. We consider the following development plan:

The first priority in year 2 will be given to the generation of the AMSR-E monthly SSS time series to cover the time period June-2002 to Sep 2011. The coherency between AMSRE SSS and CCI-L-band SSS for the common period (Jan 2010-Sep 2011) will be analysed and forced by construction.

### **3.3 Summary of the activities performed in the first half of year 2**

---

#### **3.3.1 Updated Atmospheric Correction Algorithm**

1) First, we implemented an updated version of the Wentz and Meissner (2000)'s atmospheric corrections for the C and X band frequencies. With respect the algorithm used in Reul et al., 2009, the ATBD of AMSRE data has been updated in 2012 (Wentz and Meissner, 2012) to change an important parameter of the atmospheric correction computation, namely  $T_v$ , which is representing a sea surface temperature that is typical for each water vapour value and used to evaluate most atmospheric contributions.

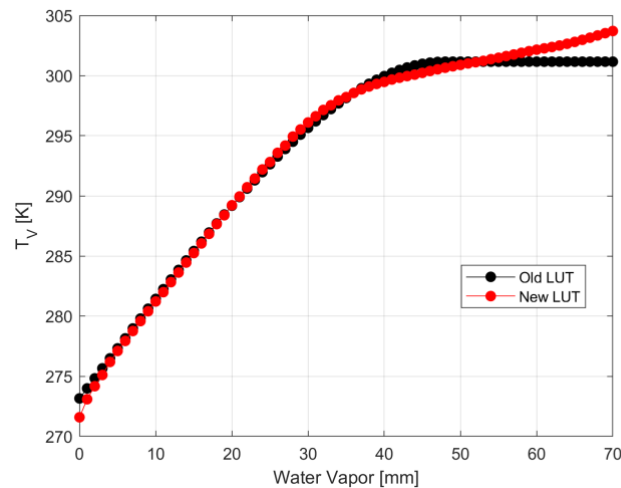


Figure 9:  $T_v$ , representing a sea surface temperature that is typical for each water vapour value.

As found (Figure 9), this parameter exhibits higher values in the new algorithm with respect the old one for High WV (WV > 50 mm).

### 3.3.2 Empirical Adjustments

An empirical adjustment part of the algorithm has been developed for the four regions described above in the first half of 2020 using an ensemble of 6 training months selected in between may 2010 and may 2011 (every other months to select the algorithm what is called hereafter the ‘training’ database. The other months being referred to as the ‘validation’ database). Despite being very robust for water vapor, SST, wind and cloud liquid water retrievals, the algorithm developed by REMSS for AMSR-E (Wentz and Messiner, 2012) is not sufficiently accurate for the low sensitivity SSS retrievals that we develop and additional adjustments for wind, SST and atmosphere impacts are needed. To provide these refining corrections, we collected residual differences between AMSR-E Tbs in C and X bands, after applying all atmospheric corrections (Wentz and Messiner, 2012), and the surface emissivity model (Dielectric constant model of Wentz and Meissner, 2012) forced by the L-band CCI data and the CCI SST, taken as a reference. These residuals have been binned as function of 1) the surface wind speed retrieved from AMSR-E, U, to provide an empirical roughness correction for each frequency 2) then as function of the surface SST from CCI to remove any potential SST-dependent biases, and finally 3), as a function of the water vapour (WV) and cloud liquid water (CLW) retrieved from AMSR-E.

#### Wind-induced emissivity correction

Differences found in average between the reference flat surface emissivity and the determined surface emissivity from AMSR-E (including roughness impacts) were binned averaged as function of the surface wind speed retrieved from AMSR-E. As found the roughness impact is not exactly the same for both C and X-band frequencies, particularly in the high and low wind speed regimes: a correction is therefore needed.

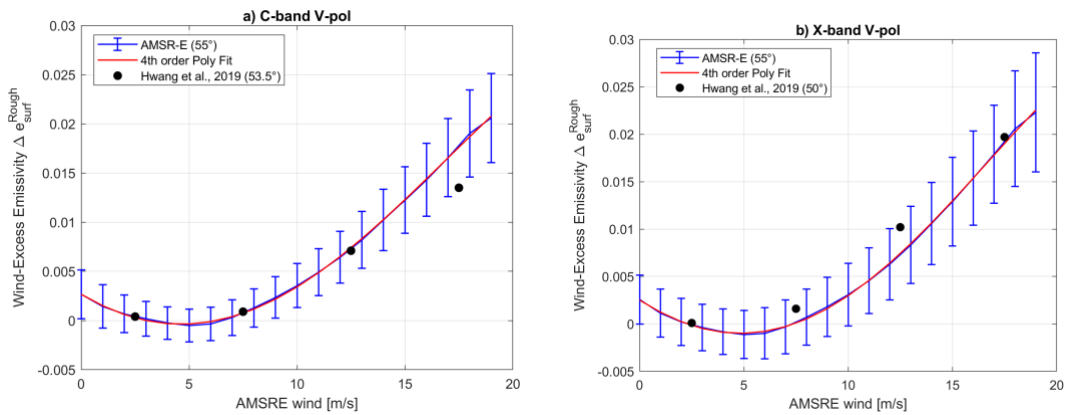


Figure 10: Wind-excess emissivity empirical GMF at C (a) and X (b) bands. The blue curves are showing the residual binned in 1 m/s binned  $\pm 1$  STD. The red curves are showing the 4<sup>th</sup> order polynomial fits used to define the algorithm GMF.

Fourth order polynomial fits were applied to determine the wind-excess emissivity empirical GMFs at each frequency (see red curves in Figure 10):

$$\Delta e_f(U) = \sum_{i=1,4} P_i U^i$$

Where  $P_i$  are fourth-order wind GMF polynomial coefficients:

f [GHz]	p	i=0	i=1	i=2	i=3	i=4
6.9	V	0.0024	-0.0014	1.5666e-04	-9.8011e-07	-5.0347e-08
10.7	V	0.0023	-0.0015	1.8440e-04	-2.4595e-06	-1.0507e-08

### SST correction

After applying the above empirical wind correction, flat ocean surface emissivity residuals (AMSR-E minus CCI-based model) were then binned as function of the SST CCI:

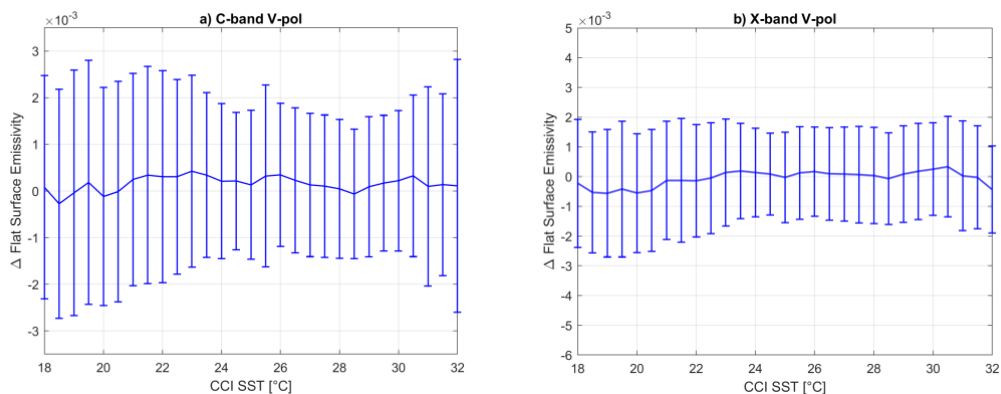


Figure 11: Flat surface emissivity residuals at C- (a) and X- (b) bands as function of the SST CCI. The blue curves are showing the residual binned in 1 m/s binned  $\pm 1$  STD.

As found, the emissivity residuals binned as function of SST for both frequencies are almost unbiased in the full SST range (18-32°C): the correction from the Wentz and Meissner (2000,2012) algorithm is therefore accurate given the independent SST CCI as input. Consequently, we decided not to apply any additional SST-dependent corrections in the algorithm.

### Water Vapor-Cloud liquid Water corrections

As a last step in developing the refining corrections, the residuals are binned as function of both water vapor and cloud liquid water. WV and CLW are geophysically connected and treated as such in the Wentz and Meissner’s algorithm. Being inter-dependent, the residuals emissivity were binned as function of both variables. The resulting observed biases with respect to the forward model of the flat surface emissivity (forced by CCI SSS & SST) are shown in Figure 12 and Figure 13. Note that the AMSRE columnar cloud liquid water values (the total cloud liquid water contained in a vertical column of atmosphere) are offset by -0.05 mm, which explains the presence of negative values.

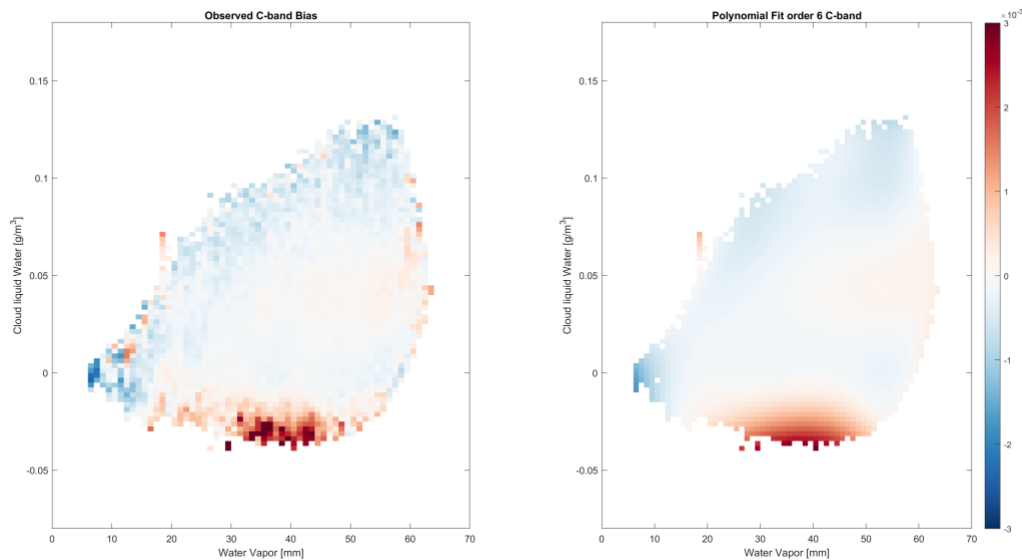


Figure 12: Observed residues of the differences between AMSRE surface emissivity at C-band and the forward model of the flat ocean surface emissivity forced with CCI SSS & SST data. The residuals are binned as function of water vapor (X-axis) and Cloud liquid water (Y-axis). Data were collected for 6 months over the four river plume regions. Right: Bi-dimensional 6th order polynomial fit.

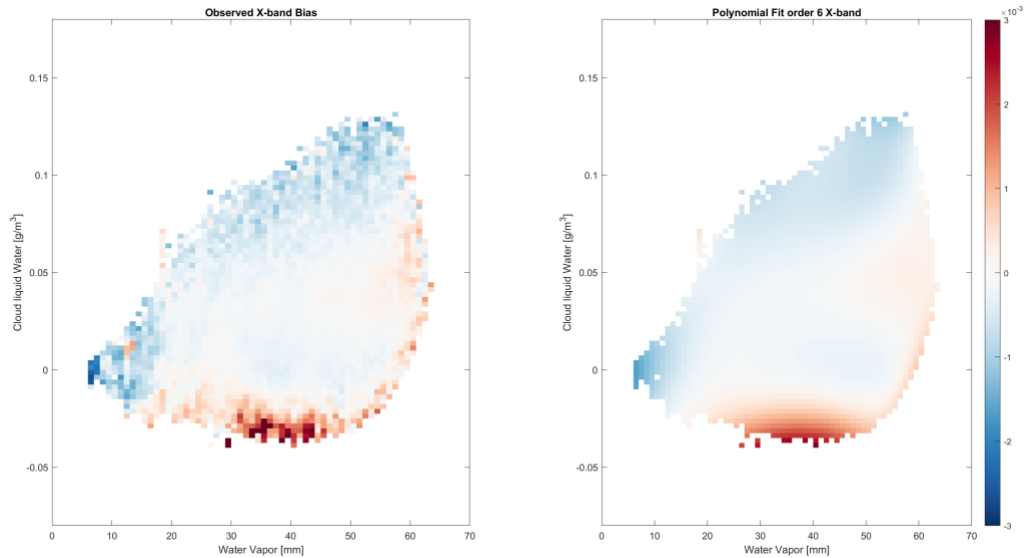


Figure 13: Observed residues of the differences between AMSRE surface emissivity at X-band and the forward model of the flat ocean surface emissivity forced with CCI SSS & SST data. The residuals are binned as function of water vapor (X-axis) and Cloud liquid water (Y-axis). Data were collected for 6 months over the four river plume regions. Right: Bi-dimensional 6th order polynomial fit.

As found, there are significant emissivity biases in the lowest and highest ranges of the CLW (all  $CLW < -0.025$  are thus too high (red) with respect the reference) but also in the extreme ranges of WV for a fixed CLW.

For each frequency, we fitted a general bivariate polynomial regression model of these biases in 6 dimensions (see right plots in Figure 12 and Figure 13).

$$\Delta e_{CLW}^{WV}(WV, CLW) = \sum_{i=0}^6 \sum_{j=0}^6 a(i,j) WV^i CLW^j$$

The coefficients  $a(i,j)$  will be provided in the next update of the ATBD.

### Salinity inversion

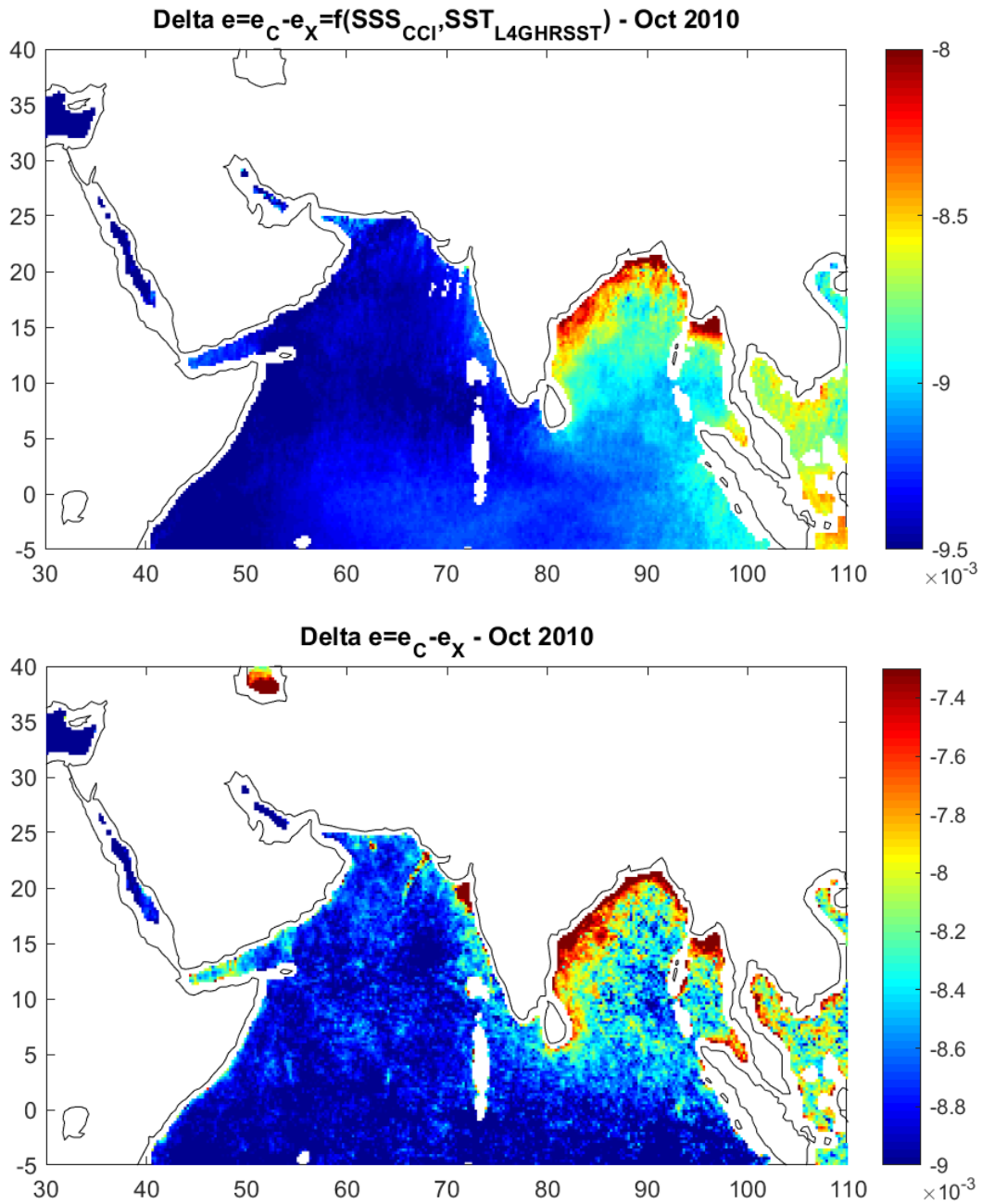


Figure 14: Monthly averaged (oct 2010) flat surface emissivity contrasts between C and X-bands (Top) from a flat ocean surface emissivity model forced by the SSS and SST CCI and (bottom) derived from AMSRE data using our algorithm.

To test the algorithm, we first focused on one month of the validation database (October 2010), and one region (North Indian ocean) which data were not used for deriving the above empirical adjustments (see Figure 14).

As Found, after applying all corrections, the monthly-averaged flat surface emissivity contrasts between C and X-bands determined from AMSR-E data (bottom) compares well with the expected/modelled signal derived from the L band CCI SSS and the CCI SST products (top). In particular, the high  $\Delta e$  regions corresponding to low SSS areas (freshwater along the Indian coasts, Irrawaddy river plume) are well matching. Differences are visible nevertheless such as in the West coast of India in the Arabian Sea or along some of the coasts (Indonesia or Sri Lanka).

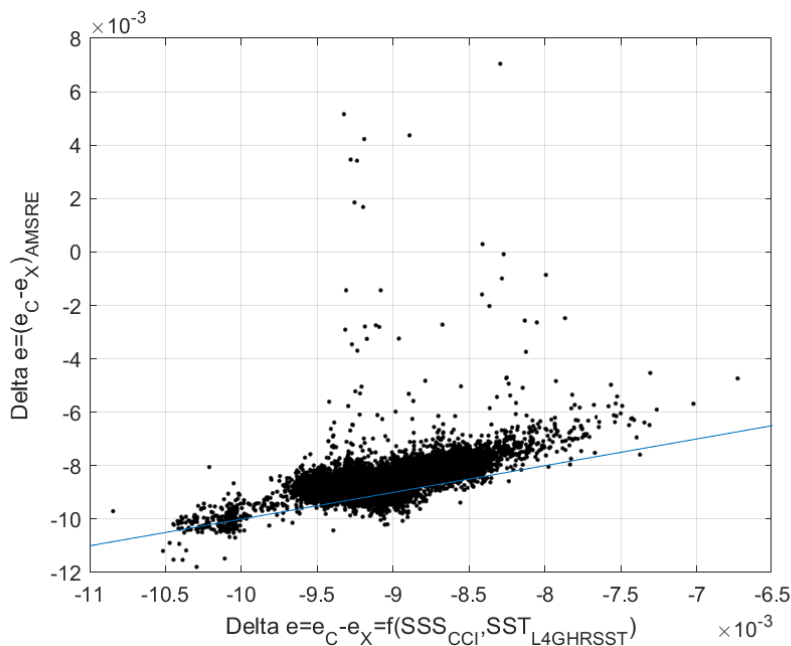


Figure 15: Monthly averaged (oct 2010) flat surface emissivity contrasts between C and X-bands derived from AMSR-E data using our algorithm as compared to the flat ocean surface emissivity model forced by the SSS and SST CCI and (bottom).

As found, after corrections, although the general signal is well detected, the flat ocean surface model differ slightly from the observations (larger dispersion in the data, biases, outliers,..). We therefore developed an empirically SSS retrieval algorithm. The training database CCI-SSS (L-band) have been binned as function of the AMSR-E estimated Flat ocean surface emissivity contrasts and the CCI SST to develop an SSS retrieval algorithm in the shape of a bivariate 6<sup>th</sup> order polynomial:

$$SSS(\Delta e, SST) = \sum_{i=0}^6 \sum_{j=0}^6 p(i, j) \Delta e^i SST^j$$

Where  $p(i, j)$  are polynomial coefficients that will be provided in the updated ATBD. The binned L-band CCI SSS as a function of the AMSR-E estimated Flat ocean surface emissivity contrasts  $\Delta e$  and CCI SST are shown in Figure 16. The model function is shown too.



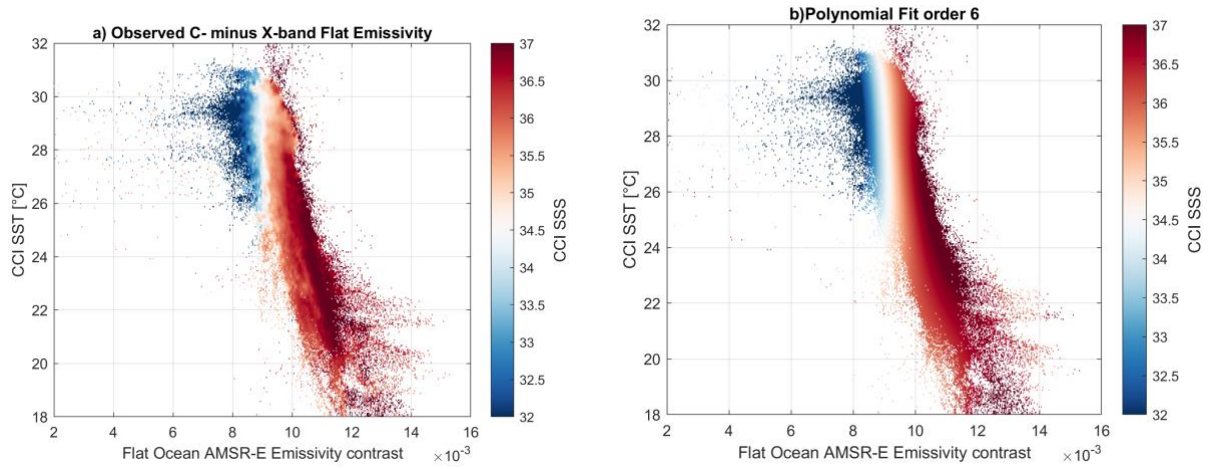


Figure 16: Left: CCI SSS (color) observed in each bin of AMSR-E flat ocean surface emissivity (x-axis) and the CCI SST (y-axis). Right: 6 order polynomial fit of the data shown in a).

### 3.3.3 AMSRE SSS development Plan for end Year 2 and year 3

First tests have been carried on to apply this SSS retrieval methodology. Example are shown in Figure 17 and Figure 18.

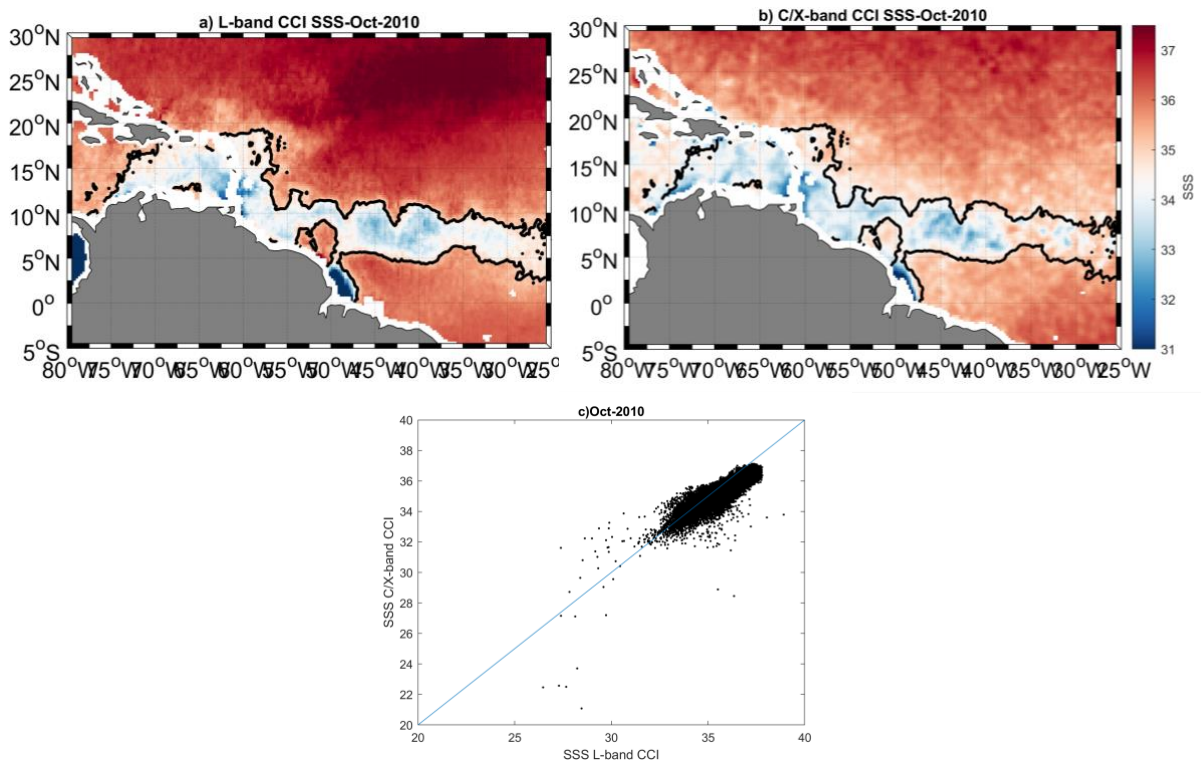


Figure 17: Monthly averaged SSS in october 2010 in the Amazon-Orinoco River plume region from SSS L-band CCI (a) and SSS from C/X band AMSR-E (right). The thick contour represent the 35 isohaline. A regression plot of AMR-E vs L-band CCI SSS is shown in c).



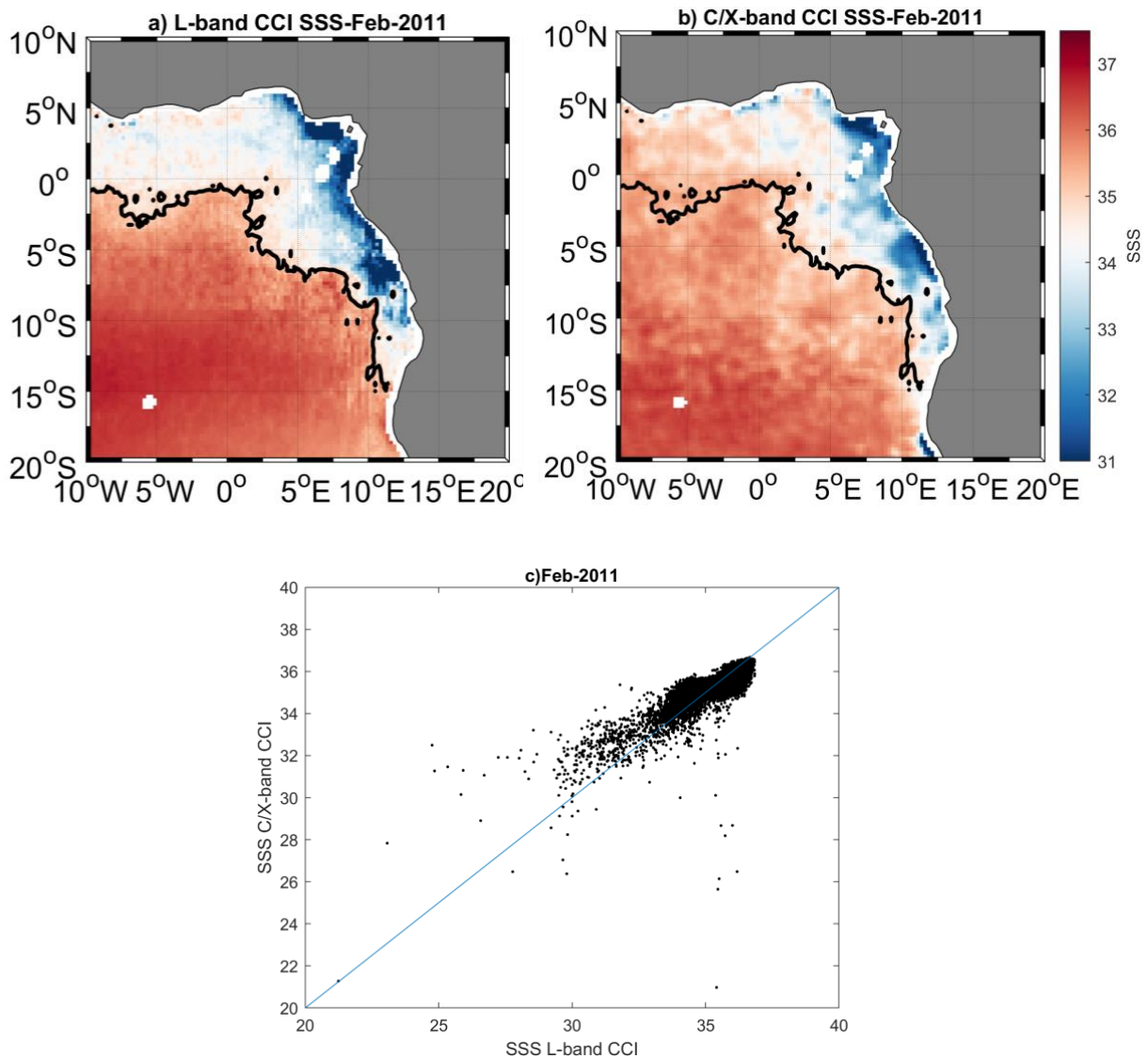


Figure 18: Monthly averaged SSS in February 2011 in the Congo-Niger River plume region from SSS L-band CCI (a) and SSS from C/X band AMSR-E (right). The thick contour represent the 35 isohaline. A regression plot of AMR-E vs L-band CCI SSS is shown in c).

The C-band algorithm will further be tested and validated against the CCI-SSS (L-band) on other regions for the same months and/or on the same region but for other months in 2010 and 2011.

The inter-region and inter-months differences between AMSR-E based and CCI-L-band SSS will then be analysed and used to ensure best coherency between these two products. We expect to deliver these products end 2020. One important next step will be to develop the filtering of outliers in the AMSR-E SSS time series used to generate the monthly products.

Another important effort will be devoted to the characterization of the AMSR-E SSS uncertainties.



### **3.4 Summary of the activities performed in year 3 and perspective for phase-2**

Most of the AMSR-E SSS retrieval algorithm have been developed and tested in first half of year 3. We are in the phase of developing the AMSR-E SSS inversion based on neural network approaches. To train the NN, the plan is to use CCI SSS v3.2 data from L-band sensors only (SMOS, Aquarius, SMAP) over the period of 21 months (jan 2010-Sep 2011) which is in common between AMSR-E & CCI SSS L band operation. The training NN will be using either the full 21 months or one of two months for the 4 splitted region separately, so that one algorithm shall be developed for each region. Some months will be used for training, some others for validation. Validation can also be conducted using in situ data collected in each region from 2002 to 2010. We plan to use a Bayesian Regularized Artificial Neural Networks to regularize the Network towards reducing bias and variance. (A high-variance state is a state when the network is overfitted). So far, we have tested NN with 2 hidden layers and 40 Neurones per layers using as input data the surface emissivity frequency differential contrasts after atmospheric corrections and the extra polynomial empirical adjustments (wind, sst, clw, wv). Retrieval tests will be conducted in phase-2 with or without these extra polynomial empirical adjustments to determine in which conditions do the NN inversion performs better. As found, one of the remaining issue is the relatively low number of training observations for the freshest SSS which lead to overestimation of SSS from AMSR-E in the freshest SSS zones. To better characterize these conditions, the distance to coast might be used as an input to the NN. An additional task will finally be to develop an error estimate for the AMSR-E SSS retrievals. Validation procedures will include in situ SSS data (Argo, TSG, XBT and moorings) gathered over the four regions back to 2002.



## 4 Summary and way forward

For the first time, SSS measurements from the three L-band satellite sensors have been merged in phase 1 to produce CCI L4 SSS time series over a decade over the global ocean. No spatial smoothing nor temporal relaxation to in-situ SSS have been introduced in order to keep as much as possible SSS interannual variability sensed by original SSS satellite measurements. On the other hand, the consistent signal between satellite SSS measured by the various sensors and under various geometries has been used to correct for systematic uncertainties. When compared with in-situ Argo SSS, the robust standard deviation (STDD\*) over the global ocean is 0.15 with monthly CCI products, the coefficient of determination is 0.97. These performances outscore the ones obtained with fields built from individual satellite measurements. The 50 x 50 km<sup>2</sup> CCI L4 SSS product provides one of the most realistic measure of SSS in very variable regions. The potential of the CCI L4 dataset for revealing new insights has been demonstrated already by various scientific studies. Focussing on the interannual variability of the SSS in the Bay of Bengal and on the signature of the river plumes, Akhil et al. (2020) found that CCI L4 SSS performed better than SSS retrieved from individual satellite sensors. In the tropical Atlantic Ocean, the CCI L4 SSS allowed to study large seasonal and interannual variability in the respective roles of salinity and temperature on the development of the tropical instability waves (TIWs) and to show that, in the top 60-m of the ocean, salinity and temperature each contribute to about 50% of the TIWs perturbation potential energy (Olivier et al., 2020). CCI L4 SSS is also used to document events of freshwater transport off the coast of Suriname and French Guyana from the shelf to the open ocean in January-March since 2010, showing that such unexpected events occurred in 7 out of 10 years (Reverdin et al., 2021).

The specifications of the CCI fields have been defined based on a poll to which 54 potential users have answered. Their requirements are, for a large part, in line with the ones formulated by other user groups and/or in other contexts, as summarized by the World Meteorological Organization (WMO) ([https://www.wmo-sat.info/oscar/variables/view/sea\\_surface\\_salinity](https://www.wmo-sat.info/oscar/variables/view/sea_surface_salinity)), or by a former user requirement analysis for future microwave radiometers operating at low frequencies (mainly L-Band) (Kerr et al. 2019). All these studies require an accuracy between 0.1 to 0.3 at spatio-temporal scales greater than 100km and one week (see [https://www.wmo-sat.info/oscar/variables/view/sea\\_surface\\_salinity](https://www.wmo-sat.info/oscar/variables/view/sea_surface_salinity)). While the spatial and temporal resolution requirements of the users and the previously mentioned studies are compatible with the Global Climate Observing System (GCOS) Implementation Plan (GCOS-200 (214); [https://library.wmo.int/doc\\_num.php?explnum\\_id=3417](https://library.wmo.int/doc_num.php?explnum_id=3417)), the GCOS uncertainty and stability requirements of 0.01 and 0.001 per decade respectively are an order of magnitude more stringent. These values, the same as the ones for subsurface in-situ data, appear very small compared to the SSS variability and the spatio-temporal undersampling of this variability by in-situ near surface salinity measurements. Even with the increase of measurements associated with the full deployment of the Argo buoy network, in-situ near surface salinity measurements do not allow to reach such accuracy over all regions of the global ocean.

The improved accuracy of the CCI L4 SSS with respect to individual sensor SSS accuracy has been made possible because individual sensor SSS products were already shown to detect consistent variabilities. For instance, D'Addezio and Subrahmanyam (2016) showed that SMOS



and Aquarius detect high SSS variability associated with the Agulhas current consistent with Argo SSS, whereas Fournier and Lee (2021) showed very consistent SMOS and SMAP SSS in river plumes areas. Yu et al. (2021) and Bingham et al. (2021) found that SSS annual and semiannual amplitudes are quite well represented over the open ocean by the satellite SSS products considered for building the CCI L4 SSS.

The methodology we have developed for building the CCI L4 dataset aims at preserving the SSS variability globally observed by satellite every few days in footprints integrated over typically 50 x 50 km<sup>2</sup>. The bias corrections are mostly based on the consistency between SSS signatures recorded by the various satellite datasets and are considering specific properties of each sensor measurements. External SSS information is considered only for calibrating the long term SSS absolute value and for estimating representativity uncertainties. The CCI+SSS approach is, therefore, upstream of the optimal interpolations which correct satellite SSS biases using in-situ SSS fields on a monthly basis or less, such as (Melnichenko et al., 2016). The CCI+SSS fields could be used as inputs to such method, as was done with SMOS data (Nardelli et al., 2016) or with SMOS and SMAP data (Kolodziejczyk et al., 2020).

Nevertheless, there is still room for improving CCI L4 SSS, their uncertainties and validation. In particular, it would be interesting to reach better stability of the CCI L4 SSS time series.

In particular, seasonal latitudinal differences remain with respect to Argo salinities, mostly before mid-2015. After mid-2015, both the inclusion of SMAP SSS and reduced SMOS SSS latitudinal biases are responsible for the improvement. The reason why SMOS SSS are more stable after mid-2015 is not entirely clear, even though a change in the SMOS calibration mode (warm Noise Injection Radiometer (NIR) calibration after November 2014) and a reduction of solar emission likely contributes to this improvement. An uncertainty on the temporal variability of SMOS SSS arises from the current use of SSS climatology in the SMOS OTT region. The interannual variability of the median SSS over the OTT region, as determined from ISAS SSS, reaches +/-0.05 during the 2010-2019 period which could be corrected. The model for the dielectric constant of seawater at L-band in cold water has also been shown to remain an issue (Boutin et al., 2021). This will be corrected in the future CCI L4 SSS release. Another source of uncertainty comes from the varying versions of ECMWF forecast fields used as priors (wind speed, SST) in the SMOS SSS retrieval. The use of the same model version for the reanalyzed fields, such as reanalyses like ERA5, could help stabilize the time series. Last, an ongoing SMOS reprocessing with a revised calibration is more stable (preliminary results) and the level 1 revised algorithm corrects part of the sun contamination at the high northern latitudes. For Aquarius SSS, remaining systematic differences have been found between ascending and descending orbits (Kao et al., 2018; Meissner et al., 2018). We have not considered correcting Aquarius SSS for systematic latitudinal seasonal biases before merging with SMOS SSS, but this should be envisioned in the future. Future studies should also pay more attention to systematic differences arising from the components of the radiative transfer models and of the prior datasets which differ between the processing chains of each of the three sensors.

The development of phase-1 CCI L4 algorithm focused on low to mid latitudes regions where satellite SSS datasets were the most mature. Recent products (Brucker et al., 2014;



Olmedo et al., 2018; Supply et al., 2020b; Tang et al., 2018) are nevertheless achieving a useful accuracy for detecting Arctic Ocean freshwater changes (Fournier et al., 2020), changes in river plumes extent (Vazquez-Cuervo et al., 2021) and their relations to wind atmospheric forcing (Tarasenko et al., 2021). Hence keeping the best potentialities demonstrated with the existing datasets associated with the three satellite missions at high latitudes will be another remaining main challenge for the future research and developments of CCI+SSS merging algorithms.

In this CCI product, no correction has been applied for rain effects on SMOS SSS products, because reliable rain estimates at hourly resolution as provided by IMERG, and as required by correction or sorting methods (Supply et al., 2020a; Supply et al., 2018), were not available before 2014, i.e., at the time of this CCI+SSS version 2 development. This effect might be non-negligible, even on monthly SSS estimates in the rainiest regions of the globe and is very likely responsible for zonal  $r$  lower than 0.95 in the tropics. In very rainy regions such as the Pacific ITCZ, Boutin et al. (2014) estimated that vertical representativeness mismatch might lead to differences between monthly salinity at a few meters depth and in the first-centimeter depth of up to 0.5 at satellite pixel level (50x50 km<sup>2</sup>). Nevertheless, this effect is very patchy, and when averaged over all longitudes, it is mostly less than 0.1, except in very abnormal conditions such as in the second part of 2015, when it reached up to 0.15 in the latitudinal band affected by the freshest anomalies (Supply et al. Ph.D. thesis 2020). During this 2015 abnormal period, modelled salinities at 10 m depth and satellite SSS in the northern tropical Pacific Ocean also differed by this order of magnitude (Hasson et al., 2018). Thus, even though this effect did not hamper the detection of 2015 large scale SSS anomalies, and that an estimate of the freshening at 1 cm depth could also be of interest for air-sea interactions studies, it will be important in future CCI L4 SSS releases to provide an estimate of CCI L4 SSS corrected from the vertical representativeness effect.

Validation with standard statistical indicators such as the ones used in phase-1 has inherent limitations. For instance, high-resolution fields might appear as having a higher RMS difference with respect to reference fields than lower resolution fields when representativity errors between reference fields and high-resolution fields are important. This effect contributes to some lower RMS difference computed with Aquarius than with CCI L4 SSS. We identified it by looking at  $r^2$ , but methodologies such as the ones developed in the high resolution modeling community (Crocker et al., 2020) could be investigated to better quantify the accuracy of high-resolution fields relative to lower resolution fields. Wavenumber spectral analysis, such as the one performed on sea surface height by (Dufau et al., 2016), should also be studied in order to validate dynamical features of SSS at various spatio-temporal scales.

The characterization of SSS variability remains challenging as, on one hand, the combination of in-situ and satellite information remains to be improved (Stammer et al., 2021); and on the other hand, regions with high SSS variability such as the river plumes or strong surface currents regions are the ones benefiting the most from the satellite information (Tranchant et al., 2019). The statistical distribution of SSS is not expected to be Gaussian (Bingham et al., 2002), especially in regions affected by fresh-water inputs, so that vertical, temporal and spatial representativity errors between in-situ and satellite measurements are not expected to be Gaussian. In particular, the SSS distributions are expected to be skewed towards low SSS values while the higher salinity parts of the SSS distributions are expected to vary much less. This leads us to adopt an adjustment of the full time series of CCI L4 SSS and ISAS SSS in fresh and very





variable regions based on a high quantile of their statistical distributions. Nevertheless, the OI assumption of Gaussian errors used here might lead to some drawbacks in fresh regions such as river plumes or rainy areas, e.g., an artificial increase (decrease) of the uncertainty during periods with decreased (increased) variability that are very difficult to quantify given the sparseness of existing in-situ measurements. For the reasons outlined above, the validation of the SSS and its uncertainty estimate is very tricky and requires extended research to go beyond the relatively crude validation performed in phase-1.

Finally, we plan future CCI+SSS updates typically once every 18 months. In future versions of the CCI products, in addition to a global product, polar products are foreseen. We also plan to develop several regional products with longer time series than the one presented in phase-1 by extending the L-band based SSS back in time to 2002 over four large and warm river plume regions (1) Mississippi; (2) Orinoco and Amazon; (3) Niger and Congo and (4) Bay of Bengal. For this, we will complement the observations provided by the suite of L-band sensors using AMSR-E lowest microwave frequency channel data (at 6.9 GHz=C-band and 10.7 GHz=X-band) acquired in warm and strongly contrasted dynamical river plume regions. In such conditions, the small SSS signal contained in C-band radiometer data is improved by differentiating the vertical polarization surface reflectance between the C and X band, minimizing SST and wind effects on the data. Monthly-averaged SSS retrievals using such approaches have been already demonstrated from AMSR-E data for the Amazon plume region (Reul et al., 2009) and HY2-A data for the freshwater runoff near the Yangtze Delta (Song and Wang, 2017). In the future, new missions such as the Copernicus Imaging Microwave Radiometer (Donlon, 2020) and the SMOS-High Resolution mission (Rodríguez-Fernández et al., 2019) will benefit from the methods and approaches pioneered by the SSS-CCI activities and extend the climate record of satellite SSS into the 2040's. Most of the AMSR-E SSS algorithm (forward model) have been developed and tested in phase 1. We are in the phase of developing the AMSR-E SSS inversion based on neural network approaches. To train the NN, the plan is to use CCI SSS v3.2 data from L-band sensors only (SMOS, Aquarius, SMAP) over the period of 21 months (jan 2010-Sep 2011) which is in common between AMSR-E & CCI SSS L band operation. The training NN will be using either the full 21 months or one of two months for the 4 splitted region separately, so that one algorithm shall be developed for each region. Some months will be used for training, some others for validation. Validation can also be conducted using in situ data collected in each region from 2002 to 2010. We plan to use a Bayesian Regularized Artificial Neural Networks to regularize the Network towards reducing bias and variance. (A high-variance state is a state when the network is overfitted). So far, we have tested NN with 2 hidden layers and 40 Neurones per layers using as input data the surface emissivity frequency differential contrasts after atmospheric corrections and the extra polynomial empirical adjustments (wind, sst, clw, wv). Retrieval tests will be conducted in phase-2 with or without these extra polynomial empirical adjustments to determine in which conditions do the NN inversion performs better. As found, one of the remaining issue is the relatively low number of training observations for the freshest SSS which lead to overestimation of SSS from AMSR-E in the freshest SSS zones. To better characterize these conditions, the distance to coast might be used as an input to the NN. An additional task will finally be to develop an error estimate for the AMSR-E SSS retrievals. Validation procedures will include in situ SSS data (Argo, TSG, XBT and moorings) gathered over the four regions back to 2002.



*Climate Change Initiative+ (CCI+)*  
*Phase 1*  
Algorithm Development Plan

**Ref.:** ESA-CCI-PRGM-EOPS-SW-17-0032

**Date:** 14/09/2021

**Version:** v3.1

**Page:** 37 of 47

*End of document*